Supplement of E&G Quaternary Sci. J., 74, 235–262, 2025 https://doi.org/10.5194/egqsj-74-235-2025-supplement © Author(s) 2025. CC BY 4.0 License.





# Supplement of

# Silts with a human touch: the shift from natural to anthropogenically controlled fluvial dynamics in the Kinzig River floodplains, southwestern Germany

Charlotte E. Engelmann et al.

Correspondence to: Charlotte E. Engelmann (charlotte.engelmann@geographie.uni-freiburg.de)

The copyright of individual parts of the supplement might differ from the article licence.

# S1. Coordinates

Table S1. Coordinates of field points in WGS 84 / UTM zone 32N, elevation in m.a.s.l..

Location	Type	Code	Northing	Easting	Elevation
Schenkenzell	Percussion drill	S1	5349850.269	453116.015	391.906
Schenkenzell	Percussion drill	S2	5349843.723	453133.6618	391.941
Schenkenzell	Percussion drill	S3	5349703.591	452980.0836	390.983
Schenkenzell	Percussion drill	S4	5349711.07	452980.0364	390.998
Schenkenzell	Percussion drill	S5	5349718.434	452979.9608	391.059
Schenkenzell	Percussion drill	S6	5349727.776	452979.9941	390.836
Schenkenzell	Hand augering	Sc01	5349694.483	452979.7138	341.768
Schenkenzell	Hand augering	Sc02	5349699.479	452979.8206	341.639
Schenkenzell	Hand augering	Sc03	5349703.467	452980.0052	341.418
Schenkenzell	Hand augering	Sc04	5349707.45	452980.1298	341.421
Schenkenzell	Hand augering	Sc05	5349710.947	452980.1881	341.418
Schenkenzell	Hand augering	Sc06	5349714.443	452980.2524	341.456
Schenkenzell	Hand augering	Sc07	5349718.439	452980.2231	341.479
Schenkenzell	Hand augering	Sc08	5349722.436	452980.2028	341.395
Schenkenzell	Hand augering	Sc09	5349724.432	452980.1821	341.331
Schenkenzell	Hand augering	Sc10	5349727.425	452980.0692	341.275
Schenkenzell	Hand augering	Sc11	5349730.397	452979.9442	341.229
Schenkenzell	Hand augering	Sc12	5349737.371	452979.7233	341.29
Schenkenzell	Hand augering	Sc13	5349742.355	452979.4658	339.906
Schenkenzell	Hand augering	Sc14	5349745.343	452979.2532	340.453
Schenkenzell	Hand augering	Sc15	5349749.309	452979.0284	341.112
Schenkenzell	Hand augering	Sc16	5349752.805	452978.9362	340.654
Schenkenzell	Hand augering	Sc17	5349755.296	452978.7966	340.631
Schenkenzell	Hand augering	Sc18	5349759.287	452978.7539	341.498
Schenkenzell	Hand augering	Sc19	5349764.282	452978.6549	342.966
Schenkenzell	Hand augering	Sc20	5349770.277	452978.5719	343.115
Schenkenzell	Hand augering	Sc21	5349776.272	452978.3653	343.043
Schenkenzell	ERT electrode	Ert_S_start	5349689.769	452979.3017	391.765
Schenkenzell	ERT electrode	Ert_S_end	5349781.19	452978.1	392.682
Schenkenzell	GPR transect	Gpr_S1_start	5349702.454	452979.803	390.896
Schenkenzell	GPR transect	Gpr_S1_end	5349736.552	452979.5424	390.782
Schenkenzell	GPR transect	Gpr_S13_start	5349702.443	452980.1597	390.931
Schenkenzell	GPR transect	Gpr_S13_end	5349736.491	452979.4447	390.794
Schenkenzell	GPR transect	Gpr_S14_start	5349733.973	452972.4022	390.867
Schenkenzell	GPR transect	Gpr_S14_end	5349704.29	452970.3838	390.916
Schenkenzell	GPR transect	Gpr_S15_start	5349707.502	452962.7758	390.927
Schenkenzell	GPR transect	Gpr_S15_end	5349735.204	452966.6443	390.797
Schenkenzell	GPR transect	Gpr_S16_start	5349734.332	452961.3143	390.776
Schenkenzell	GPR transect	Gpr_S16_end	5349708.199	452954.8788	390.999
Schenkenzell	GPR transect	Gpr_S17_start	5349708.96	452948.5635	390.889
Schenkenzell	GPR transect	Gpr_S17_end	5349735.633	452954.9668	390.683

0.1.1.11	CDD	G (10 )	5240504 055	452005 5744	200.000
Schenkenzell	GPR transect	Gpr_S18_start	5349704.977	452985.5744	390.969
Schenkenzell	GPR transect	Gpr_S18_end	5349736.733	452984.5029	390.779
Schenkenzell	GPR transect	Gpr_S19_start	5349737.865	452989.9716	390.872
Schenkenzell	GPR transect	Gpr_S19_end	5349705.435	452993.1333	391.040
Schenkenzell	GPR transect	Gpr_S20_start	5349707.941	453001.2937	391.125
Schenkenzell	GPR transect	Gpr_S20_end	5349740.144	452999.9637	390.898
Schenkenzell	GPR transect	Gpr_S21_start	5349740.729	453005.3512	390.963
Schenkenzell	GPR transect	Gpr_S21_end	5349707.446	453009.2163	391.138
Schenkenzell	GPR transect	Gpr_S22_start	5349712.426	453019.721	391.145
Schenkenzell	GPR transect	Gpr_S22_end	5349720.902	452932.6709	390.724
Schenkenzell	GPR transect	Gpr_S23_start	5349728.002	452934.8618	390.645
Schenkenzell	GPR transect	Gpr_S23_end	5349724.534	453018.4651	390.999
Schenkenzell	GPR transect	Gpr_S25_start	5349835.09	453108.2128	391.819
Schenkenzell	GPR transect	Gpr_S25_end	5349808.601	453200.0578	392.692
Schenkenzell	GPR transect	Gpr_S26_start	5349819.137	453202.2626	393.021
Schenkenzell	GPR transect	Gpr_S26_end	5349850.806	453113.3845	391.937
Schenkenzell	GPR transect	Gpr_S27_start	5349977.412	453115.9456	392.918
Schenkenzell	GPR transect	Gpr_S27_end	5349911.762	453136.1361	392.196
Schenkenzell	GPR transect	Gpr_S28_start	5349905.861	453142.1624	392.329
Schenkenzell	GPR transect	Gpr_S28_end	5349805.862	453102.2075	391.738
Schenkenzell	GPR transect	Gpr_S29_start	5349790.606	453133.1796	391.833
Schenkenzell	GPR transect	Gpr_S29_end	5349901.884	453169.2853	392.659
Oberwolfach	Percussion drill	O1	5356403.121	445629.0441	408.570
Oberwolfach	Percussion drill	O2	5356407.764	445630.7397	408.543
Oberwolfach	Percussion drill	O3	5356398.524	445635.1354	408.698
Oberwolfach	Percussion drill	O4	5356389.533	445643.0192	408.906
Oberwolfach	Percussion drill	O5	5356393.857	445639.3691	408.824
Oberwolfach	Hand augering	Ob01	5356408.23	445626.5998	358.649
Oberwolfach	Hand augering	Ob02	5356405.678	445628.9781	359.010
Oberwolfach	Hand augering	Ob03	5356404.218	445630.2796	359.097
Oberwolfach	Hand augering	Ob04	5356400.84	445633.2261	359.159
Oberwolfach	Hand augering	Ob05	5356398.587	445635.2178	359.191
Oberwolfach	Hand augering	Ob06	5356396.29	445637.2346	359.224
Oberwolfach	Hand augering	Ob07	5356393.697	445639.5138	359.301
Oberwolfach	Hand augering	Ob08	5356389.533	445643.1268	359.352
Oberwolfach	Hand augering	Ob09	5356386.556	445645.7589	359.315
Oberwolfach	Hand augering	Ob10	5356382.791	445649.0444	359.331
Oberwolfach	Hand augering	Ob11	5356379.038	445652.3503	359.287
Oberwolfach	Hand augering	Ob12	5356375.286	445655.651	359.376
Oberwolfach	Hand augering	Ob13	5356373.022	445657.6197	359.684
Oberwolfach	Hand augering	Ob14	5356370.039	445660.2784	360.709
Oberwolfach	Hand augering	Ob15	5356367.032	445662.9137	363.282
Oberwolfach	Hand augering	Ob16	5356364.033	445665.5598	364.907
Oberwolfach	Hand augering	Ob17	5356357.989	445670.7937	367.127
Oberwolfach	Hand augering	Ob18	5356351.883	445675.9641	368.545
Oberwolfach	Hand augering  Hand augering	Ob19	5356347.274	445679.7898	370.442
OUCI WUIIACII	mand augemig	0017	3330341.214	++2017.1070	510.442

Oberwolfach	Hand augering	Ob20	5356343.379	445682.9221	371.325
Oberwolfach	ERT electrode	Ert_O_start	5356410.411	445624.4806	407.352
Oberwolfach	ERT electrode	Ert_O_end	5356341.385	445684.2634	421.879
Oberwolfach	GPR transect	Gpr_O30_start	5356407.507	445626.9604	408.246
Oberwolfach	GPR transect	Gpr_O30_end	5356354.371	445672.8398	417.547
Oberwolfach	GPR transect	Gpr_O31_start	5356359.576	445647.8661	408.503
Oberwolfach	GPR transect	Gpr_O31_end	5356382.238	445615.393	408.027
Oberwolfach	GPR transect	Gpr_O32_start	5356361.824	445606.5197	407.942
Oberwolfach	GPR transect	Gpr_O32_end	5356340.177	445632.2367	408.339
Oberwolfach	GPR transect	Gpr_O33_start	5356307.426	445583.0397	407.810
Oberwolfach	GPR transect	Gpr_O33_end	5356409.051	445650.6562	409.011
Oberwolfach	GPR transect	Gpr_O34_start	5356398.798	445660.7745	409.109
Oberwolfach	GPR transect	Gpr_O34_end	5356332.563	445625.557	408.272
Wolfach	Percussion drill	W1	5347719.193	441350.8517	299.751
Wolfach	Percussion drill	W2	5347710.426	441346.6672	299.269
Wolfach	Percussion drill	W3	5347693.024	441341.3408	299.333
Wolfach	Percussion drill	W4	5347631.617	441319.096	298.993
Wolfach	Hand augering	Wo01	5347625.381	441316.9922	249.278
Wolfach	Hand augering	Wo02	5347631.549	441319.1276	249.504
Wolfach	Hand augering	Wo03	5347639.566	441321.9542	249.735
Wolfach	Hand augering	Wo04	5347647.415	441324.6403	249.936
Wolfach	Hand augering	Wo05	5347653.738	441326.8496	249.745
Wolfach	Hand augering	Wo06	5347660.828	441329.307	249.935
Wolfach	Hand augering	Wo07	5347666.456	441331.389	249.968
Wolfach	Hand augering	Wo08	5347672.075	441333.4947	249.976
Wolfach	Hand augering	Wo09	5347678.451	441335.8499	250.020
Wolfach	Hand augering	Wo10	5347684.741	441338.1448	249.963
Wolfach	Hand augering	Wo11	5347693.206	441341.1719	249.814
Wolfach	Hand augering	Wo12	5347700.267	441343.6966	250.207
Wolfach	Hand augering	Wo13	5347710.098	441347.3533	249.786
Wolfach	Hand augering	Wo14	5347718.998	441350.6369	250.24
Wolfach	Hand augering	Wo15	5347724.141	441352.5358	250.05
Wolfach	Hand augering	Wo16	5347729.77	441354.638	250.033
Wolfach	Hand augering	Wo17	5347736.797	441357.2502	250.549
Wolfach	Hand augering	Wo18	5347743.81	441359.8932	250.969
Wolfach	ERT electrode	Ert_W_start	5347616.814	441314.156	296.821
Wolfach	ERT electrode	Ert_W_end	5347750.274	441362.2726	300.987
Wolfach	GPR transect	Gpr_W_0	5347644.359	441325.3248	299.311
Wolfach	GPR transect	Gpr_W_25	5347668.025	441333.7005	299.476
Wolfach	GPR transect	Gpr_W_50	5347691.516	441342.1268	299.342
Wolfach	GPR transect	Gpr_W_75	5347715.003	441350.7579	299.520
Wolfach	GPR transect	Gpr_W_100	5347738.508	441359.2211	300.217
Wolfach	GPR transect	Gpr_Q75_15	5347720.116	441336.5284	299.494
Wolfach	GPR transect	Gpr_Q25_15	5347673.094	441319.7517	299.441

# S2. Sediment dating

# S2.1. Sample handling

After cutting the in liners under red-light conditions, plastic foil, aluminium foil, and light-blocking bags covered the luminescence halves. Further preparation of the core-halves included cleaning by scraping away surface material and cutting off outer sections to remove the majority of potential contaminations as insertion of new percussion drillings moves top-material down the profile.

# S2.2. Sample preparation Equivalent Dose (De)

Sample preparation for determination of the Equivalent Dose ( $D_e$ ) required wet sieving using tap water (100-200  $\mu$ m; if too little material, 63-200  $\mu$ m), treatment with 20 % HCl to remove carbonates, and 15 % H<sub>2</sub>O<sub>2</sub> to destroy organic matter. Then, heavy liquid separation was applied firstly using 2.7 g/cm<sup>3</sup> LST heavy liquid to separate heavy minerals from quartz and feldspar, then using 2.58 g/cm<sup>3</sup> LST to separate quartz from K-feldspar, as the luminescence signal in quartz is reset faster and fading is less of an issue. Subsequently, quartz grains were etched with 40 % HF for 45 min to both remove the outer layer that received alpha irradiation and destroy remaining feldspar. The samples were finally treated with 20 % HCl to dissolve fluorites. All steps were separated by rinsing with distilled water and drying. Measurements were carried out on a Freiberg Instruments Standard device using the SAR protocol using a preheat at 180 °C for 10 s and stimulation with green LEDs (525 nm) for 50 s at 125 °C. A sigmab value of 0.2 was used based on the range of values found in fluvial material and experience to focus on the more central and lower De values (Fuchs et al., 2015).

# S2.3. Sample preparation dose rate (D<sub>e</sub>), estimation cosmic dose rates, calculations dose rate and ages

Sample preparation for determining the dose rate ( $D_0$ ) required drying for dry sieving to < 2 mm, homogenisation using a mortar and pestle, and material storage in an air-tight container for 3-4 weeks before measurement. The activity of different isotopes occurred similar to the procedures given in Preusser et al. (2023).

Cosmic dose rates were estimated regarding geographic position, altitude, and sampling depth.

Dose rate and ages were calculated using ADELEv2017 (Degering and Degering, 2020) using an average water content of 20  $\pm$  5 % (dry weight) as based on the sample characteristics and water content analyses as presented by Preusser et al., 2023.

## S2.4. Radiocarbon sample preparation and interpretation

Peat samples were dried at 60 °C for several days before further pre-treatment to extract datable material.

At the laboratory, wood samples underwent cellulose extraction and graphitisation, whereas peat was treated with a standard acid-base-acid (ABA) method for carbonate and secondary organic acid removal, then neutralisation of the solution.

The W1 sample was likely a root penetrating the soil column and the Sc13 wood sample stored in the currently water-holding palaeochannel.

# S2.5. Sedimentation rate computation and uncertainties

Several challenges impede the establishment of a robust depositional chronology of fluvial deposits. Among these are external factors affecting depositional processes like ag times as introduced by intermittent storage and retarded reworking along the sediment cascade (Trimble, 1999). It is shown that anthropogenically triggered enhanced sedimentation can lag behind the actual anthropogenic landscape impact (e.g., Lang and Honscheidt, 1999; Lang, 2003; Rommens et al., 2006; Fuchs et al., 2010; Larsen et al., 2013; Verstraeten et al., 2017). Additionally, sediments that already passed several sedimentary cycles would become more susceptible to store luminescence signals. Regardless, luminescence dating precision should not be impeded if luminescence signals are strong enough and the material is equally likely to be transported and deposited within the fluvial system.

Ultimately, computing sedimentation rates is challenging given the dynamic character of floodplains that allow for sediment reworking that result in phases of aggradation, reworking, and removal. Additionally, the impact of microtopography, morphology and hydraulic conditions of floodplains highly affect the stochastic sediment transport and deposition and with that reworking itself (Walling and He, 1998). Using robust methods such as OSL dating of quartz grains to compute the time since sediment deposition, considering partial bleaching of fluvial sediments, does however form a basis of computing sedimentation rates.

The sedimentation rate (SR) is computed as follows:

$$SR = \frac{depth\ layer}{age\ layer}$$

for each age layer (Table 2) with "depth layer" as the depth between the deep and shallow dating sample depths and "age layer" as the total time between the deep and shallow age.

Using formulas on propoagation of uncertainties, the error in the age of the layers in the main cores as separated by the luminescence sample depths and ages was computed as follows:

$$\sigma_{AL} = \sqrt{\sigma_{LA}^2 + \sigma_{UA}^2}$$

for each age layer (Table 2) with  $\sigma_{AL}$  the uncertainty of the age layer,  $\sigma_{LA}$  the uncertainty of the lower OSL age, and  $\sigma_{UA}$  the uncertainty of the upper OSL age.

Then, the error in the sedimentation rate over these layers was computed as follows:

$$\sigma_{SR} = SR * \sqrt{\frac{\sigma_{DL}^2}{DL}^2 + \frac{\sigma_{AL}^2}{AL}}$$

for each age layer (Table 2) with  $\sigma_{SR}$  the uncertainty of the sedimentation rate,  $\sigma_{DL}$  the uncertainty of the depth of the layer, DL the depth of the layer,  $\sigma_{AL}$  the uncertainty of the age layer, and AL the age of the layer. The uncertainty of the depth of the layer was taken as zero.

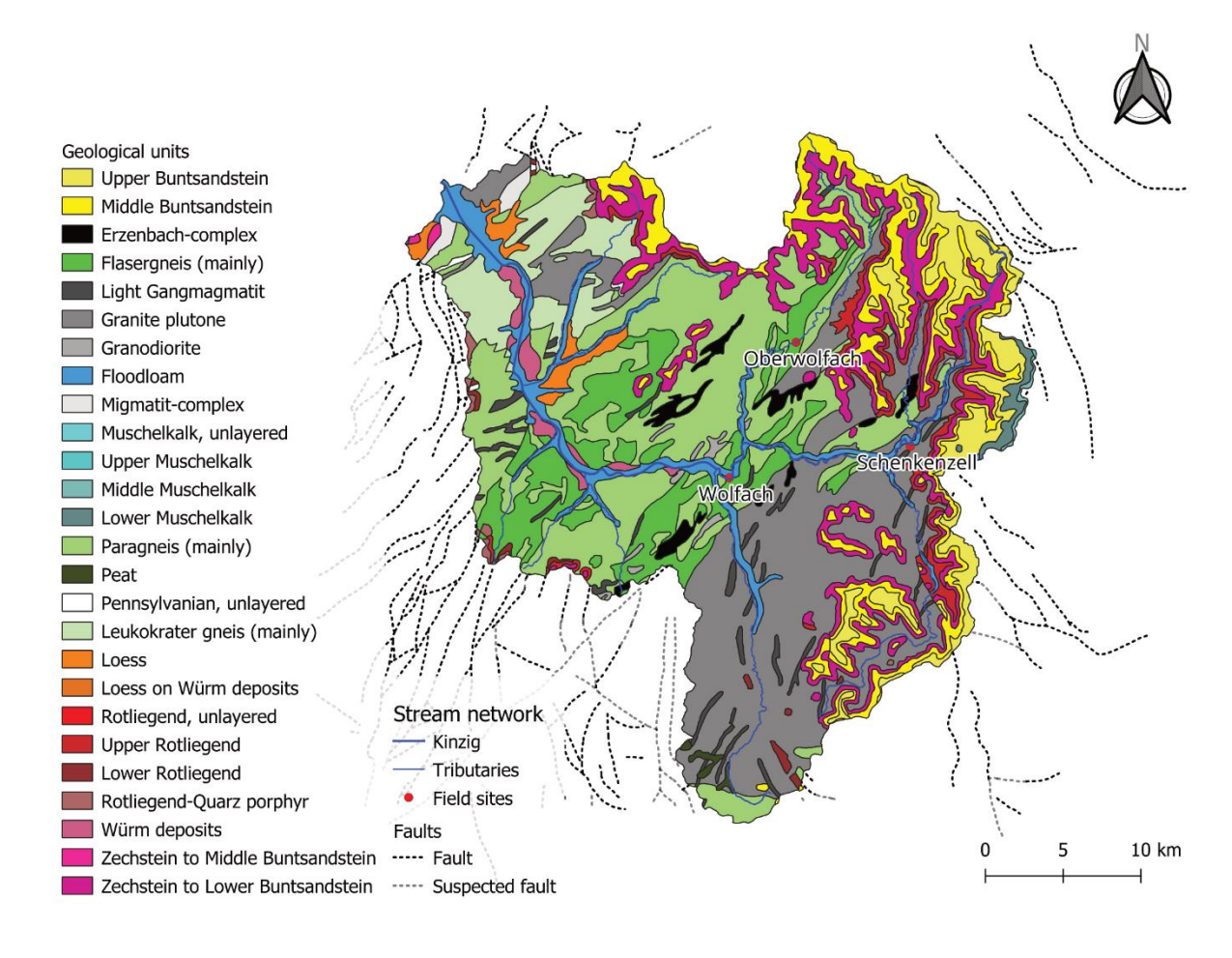


Figure S1. Geological map of the catchment showing the geological units with fault borders and the stream network including field sites. Units from LGRB (2024).

Table S2. Calibrated radiocarbon dating results (plot in Fig. S2) based on Ramsey (2009) given in years before 1950 (cal B.P.) with an uncertainty of one standard deviation. Ages corrected for isotopic fractination using the measured 13/12C-ratio. Ages presented unrounded. Equipment used for analysis: Single stage accelerator mass spectrometer (SSAMS, NEC, USA), Automated Graphitization Equipment AGE-3 (Ionplus AG, Zürich). Method of analysis: Sediment samples underwent acid washing to remove carbonates. IAEA C3, IAEA C9, and NIST-OXII were used as reference materials. \* = date out of range; \*\*\* = date may extend out of range; \*\*\* = date probably out of range.

Core	Depth (m bs)	Material	Laboratory code	Radiocarbon age (B.P.)	Calibra (cal B.l		arbon age	pMC
					Mean	from 95.4 %	to 95.4%	
W1	0.61	Wood	FTMC-PF62-1*	-1468 ± 28			-1635	$120.05 \pm 0.42$
Sc10	1.57	Peat	FTMC-PF62-2	$809 \pm 29$	712	771	675	$90.42 \pm 0.32$
Sc13	0.58	Wood	FTMC-PF62- 3**,***	119 ± 28	130	270	10	$98.53 \pm 0.35$
Sc18	0.47	Peat	FTMC-PF62-4***	$-25 \pm 29$	128	254	40	$100.31 \pm 0.36$

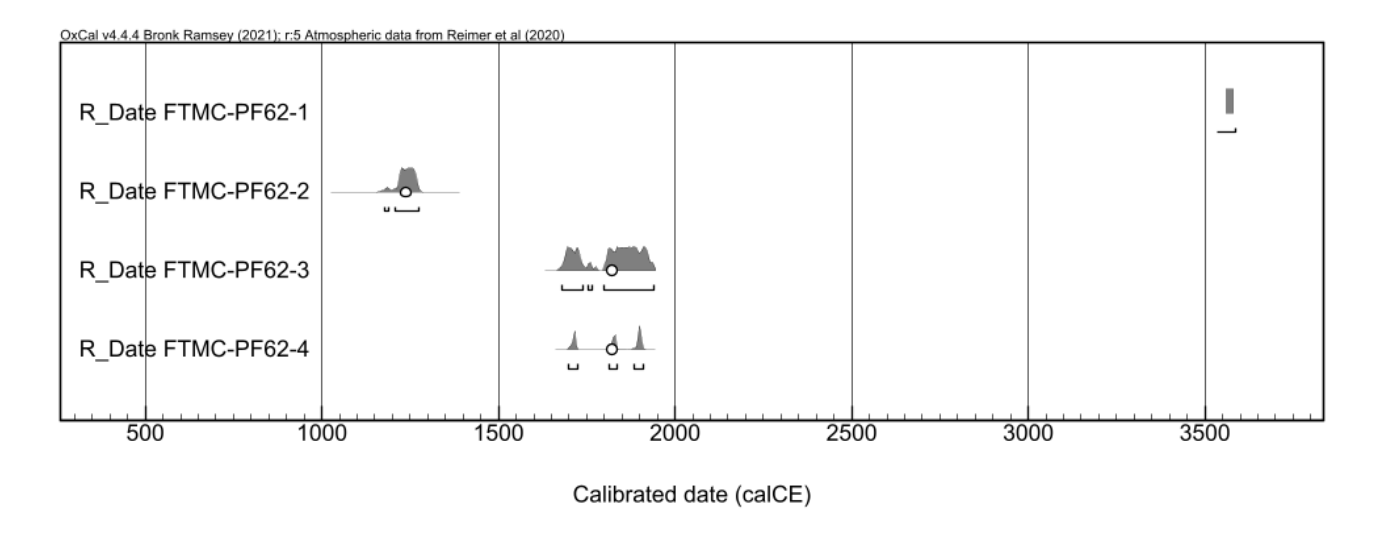


Figure S2. OxCal plot of radiocarbon samples (values in Table S2) dates showing the likelihoods (probability density functions), 95.4% range (brackets below distribution plots), and mean values (dots) (Ramsey, 2009).

Table S3. Approximated IRSL ages including the mean grain-size (Mz), dose rate (D0), palaeodose (DP), and palaeodose error (DPe).

$\begin{array}{c} W1 & 0.14 & 10.9 & 3.73 & 4.72 & 0.10 & 2.53 \pm 0.06 & 1.27 \pm 0.03 & 0.84 \pm 0.02 \\ W1 & 0.26 & 11.13 & 3.73 & 4.45 & 0.10 & 2.39 \pm 0.06 & 1.19 \pm 0.03 & 0.80 \pm 0.02 \\ W1 & 0.52 & 30.34 & 3.67 & 3.62 & 0.073 & 1.97 \pm 0.04 & 0.98 \pm 0.02 & 0.66 \pm 0.01 \\ W1 & 0.64 & 18.84 & 3.71 & 3.27 & 0.081 & 1.76 \pm 0.04 & 0.88 \pm 0.02 & 0.59 \pm 0.01 \\ W1 & 1.16 & 19.83 & 3.7 & 26.90 & 0.57 & 14.53 \pm 0.31 & 7.26 \pm 0.15 & 4.84 \pm 0.10 \\ W1 & 1.27 & 168.23 & 3.29 & 27.80 & 0.59 & 16.91 \pm 0.36 & 8.46 \pm 0.18 & 5.64 \pm 0.12 \\ W1 & 1.61 & 197.06 & 3.21 & 41.68 & 0.89 & 25.99 \pm 0.55 & 12.99 \pm 0.28 & 8.66 \pm 0.18 \\ W2 & 0.07 & 17.82 & 3.71 & 3.09 & 0.073 & 1.67 \pm 0.04 & 0.83 \pm 0.02 & 0.56 \pm 0.01 \\ W2 & 0.21 & 18.17 & 3.71 & 2.67 & 0.066 & 1.44 \pm 0.04 & 0.72 \pm 0.02 & 0.48 \pm 0.01 \\ W2 & 0.35 & 13.87 & 3.72 & 6.34 & 0.14 & 3.41 \pm 0.08 & 1.70 \pm 0.04 & 1.14 \pm 0.03 \\ W2 & 0.48 & 14.21 & 3.72 & 8.79 & 0.19 & 4.72 \pm 0.10 & 2.36 \pm 0.05 & 1.58 \pm 0.03 \\ W2 & 0.62 & 50.16 & 3.62 & 13.00 & 0.28 & 7.19 \pm 0.15 & 3.59 \pm 0.08 & 2.40 \pm 0.05 \\ W2 & 1.13 & 426.46 & 2.56 & 32.19 & 0.68 & 25.10 \pm 0.53 & 12.55 \pm 0.27 & 8.37 \pm 0.18 \\ W2 & 1.25 & 348.86 & 2.78 & 32.39 & 0.69 & 23.29 \pm 0.50 & 11.64 \pm 0.25 & 7.76 \pm 0.17 \\ W3 & 1.1 & 112.28 & 3.44 & 73.20 & 1.56 & 42.50 \pm 0.90 & 21.25 \pm 0.45 & 14.17 \pm 0.34 \\ W4 & 0.67 & 24.7 & 3.69 & 36.77 & 0.79 & 19.93 \pm 0.43 & 9.97 \pm 0.21 & 66.44 \pm 0.14 \\ S1 & 0.14 & 52.87 & 3.61 & 17.57 & 0.37 & 9.73 \pm 0.21 & 4.87 \pm 0.10 & 3.24 \pm 0.07 \\ S4 & 1.27 & 10.45 & 3.73 & 12.95 & 0.27 & 6.95 \pm 0.15 & 3.47 \pm 0.10 & 3.24 \pm 0.07 \\ S5 & 0.06 & 25.22 & 3.69 & 10.16 & 0.23 & 5.51 \pm 0.12 & 2.75 \pm 0.06 & 1.84 \pm 0.04 \\ S5 & 0.18 & 34.96 & 3.66 & 2.52 & 0.051 & 1.38 \pm 0.03 & 0.69 \pm 0.01 & 0.46 \pm 0.01 \\ S5 & 0.41 & 29.92 & 3.68 & 5.18 & 0.12 & 2.82 \pm 0.06 & 1.41 \pm 0.03 & 0.94 \pm 0.02 \\ S5 & 0.53 & 51.68 & 3.61 & 8.28 & 0.18 & 4.58 \pm 0.10 & 2.29 \pm 0.05 & 1.53 \pm 0.08 \\ S5 & 0.65 & 37.45 & 3.65 & 12.89 & 0.28 & 7.06 \pm 0.15 & 3.53 \pm 0.08 & 2.35 \pm 0.05 \\ S5 & 0.65 & 37.45 & 3.65 & 12.89 & 0.28 & 7.76 \pm 0.16 & 3.88 \pm 0.08 & 2.59 \pm 0.05 \\ S5 & 0.65 & 37.$	Core	Depth (m bs)	$M_{z}\left(\mu m\right)$	D <sub>0</sub> (Gy/ka)	$D_{p}\left( Gy\right)$	$D_{Pe}\left( Gy\right)$	Age ± error (ka)		
$\begin{array}{c} W1 & 0.14 & 10.9 & 3.73 & 4.72 & 0.10 & 2.53 \pm 0.06 & 1.27 \pm 0.03 & 0.84 \pm 0.02 \\ W1 & 0.26 & 11.13 & 3.73 & 4.45 & 0.10 & 2.39 \pm 0.06 & 1.19 \pm 0.03 & 0.80 \pm 0.02 \\ W1 & 0.52 & 30.34 & 3.67 & 3.62 & 0.073 & 1.97 \pm 0.04 & 0.98 \pm 0.02 & 0.66 \pm 0.01 \\ W1 & 0.64 & 18.84 & 3.71 & 3.27 & 0.081 & 1.76 \pm 0.04 & 0.88 \pm 0.02 & 0.59 \pm 0.01 \\ W1 & 1.16 & 19.83 & 3.7 & 26.90 & 0.57 & 14.53 \pm 0.31 & 7.26 \pm 0.15 & 4.84 \pm 0.10 \\ W1 & 1.27 & 168.23 & 3.29 & 27.80 & 0.59 & 16.91 \pm 0.36 & 8.46 \pm 0.18 & 5.64 \pm 0.12 \\ W1 & 1.61 & 197.06 & 3.21 & 41.68 & 0.89 & 25.99 \pm 0.55 & 12.99 \pm 0.28 & 8.66 \pm 0.18 \\ W2 & 0.07 & 17.82 & 3.71 & 3.09 & 0.073 & 1.67 \pm 0.04 & 0.83 \pm 0.02 & 0.56 \pm 0.01 \\ W2 & 0.21 & 18.17 & 3.71 & 2.67 & 0.066 & 1.44 \pm 0.04 & 0.72 \pm 0.02 & 0.48 \pm 0.01 \\ W2 & 0.35 & 13.87 & 3.72 & 6.34 & 0.14 & 3.41 \pm 0.08 & 1.70 \pm 0.04 & 1.14 \pm 0.03 \\ W2 & 0.48 & 14.21 & 3.72 & 8.79 & 0.19 & 4.72 \pm 0.10 & 2.36 \pm 0.05 & 1.58 \pm 0.03 \\ W2 & 0.62 & 50.16 & 3.62 & 13.00 & 0.28 & 7.19 \pm 0.15 & 3.59 \pm 0.08 & 2.40 \pm 0.05 \\ W2 & 1.13 & 426.46 & 2.56 & 32.19 & 0.68 & 25.10 \pm 0.53 & 12.55 \pm 0.27 & 8.37 \pm 0.18 \\ W2 & 1.25 & 348.86 & 2.78 & 32.39 & 0.69 & 33.29 \pm 0.53 & 11.64 \pm 0.25 & 7.76 \pm 0.17 \\ W3 & 1.1 & 112.28 & 3.44 & 73.20 & 1.56 & 42.50 \pm 0.90 & 21.25 \pm 0.45 & 14.17 \pm 0.33 \\ W4 & 0.67 & 24.7 & 3.69 & 36.77 & 0.79 & 19.93 \pm 0.43 & 9.97 \pm 0.21 & 66.44 \pm 0.14 \\ S2.87 & 3.61 & 17.57 & 0.37 & 9.73 \pm 0.21 & 4.87 \pm 0.10 & 3.24 \pm 0.07 \\ S4 & 0.51 & 52.66 & 3.61 & 13.92 & 0.31 & 7.71 \pm 0.17 & 3.85 \pm 0.09 & 2.57 \pm 0.06 \\ S4 & 1.27 & 10.45 & 3.73 & 12.95 & 0.27 & 6.95 \pm 0.15 & 3.47 \pm 0.10 & 3.24 \pm 0.07 \\ S5 & 0.06 & 25.22 & 3.69 & 10.16 & 0.23 & 5.51 \pm 0.12 & 2.75 \pm 0.06 & 1.84 \pm 0.04 \\ S5 & 0.18 & 34.96 & 3.66 & 2.52 & 0.051 & 1.38 \pm 0.03 & 0.69 \pm 0.01 & 0.46 \pm 0.01 \\ S5 & 0.18 & 34.96 & 3.66 & 2.52 & 0.051 & 1.38 \pm 0.03 & 0.69 \pm 0.01 & 0.46 \pm 0.01 \\ S5 & 0.41 & 29.92 & 3.68 & 5.18 & 0.12 & 2.82 \pm 0.06 & 1.41 \pm 0.03 & 0.94 \pm 0.02 \\ S5 & 0.53 & 51.68 & 3.61 & 8.28 & 0.18 & 4.58 \pm 0.10 & 2.29 \pm 0.05 & 1.53 \pm 0.05 \\ S5 & 0.65 & 37.45 & 3.65 & $							Minimum	Average	Maximum
$\begin{array}{c} W1 & 0.26 \\ W1 & 0.52 \\ W1 & 0.52 \\ \end{array} \begin{array}{c} 30.34 & 3.67 \\ 3.62 & 0.073 \\ \end{array} \begin{array}{c} 1.97 \pm 0.04 \\ 0.98 \pm 0.02 \\ \end{array} \begin{array}{c} 0.66 \pm 0.01 \\ 0.88 \pm 0.02 \\ 0.66 \pm 0.01 \\ \end{array} \begin{array}{c} 0.64 \\ 18.84 \\ 3.71 \\ \end{array} \begin{array}{c} 3.27 \\ 0.081 \\ \end{array} \begin{array}{c} 0.081 \\ 1.76 \pm 0.04 \\ 0.88 \pm 0.02 \\ 0.59 \pm 0.01 \\ \end{array} \begin{array}{c} 0.52 \pm 0.01 \\ 0.59 \pm 0.01 \\ \end{array} \begin{array}{c} 0.66 \pm 0.01 \\ 0.88 \pm 0.02 \\ 0.59 \pm 0.01 \\ \end{array} \begin{array}{c} 0.59 \pm 0.01 \\ 0.57 \\ \end{array} \begin{array}{c} 1.16 \\ 1.16 \\ \end{array} \begin{array}{c} 1.16 \\ 1.9.83 \\ 3.7 \\ \end{array} \begin{array}{c} 2.6.90 \\ 0.57 \\ 0.57 \\ \end{array} \begin{array}{c} 1.4.53 \pm 0.31 \\ 0.59 \\ 16.91 \pm 0.36 \\ \end{array} \begin{array}{c} 8.46 \pm 0.18 \\ 0.18 \\ \end{array} \begin{array}{c} 4.84 \pm 0.10 \\ 0.88 \pm 0.02 \\ 0.59 \pm 0.15 \\ \end{array} \begin{array}{c} 4.84 \pm 0.10 \\ 0.88 \pm 0.02 \\ 0.59 \pm 0.15 \\ \end{array} \begin{array}{c} 4.84 \pm 0.10 \\ 0.83 \pm 0.02 \\ 0.56 \pm 0.01 \\ \end{array} \begin{array}{c} 0.52 \pm 0.15 \\ 0.07 \\ 0.07 \\ \end{array} \begin{array}{c} 1.16 \\ 1.97.06 \\ 3.21 \\ 3.71 \\ 3.09 \\ 0.07 \\ \end{array} \begin{array}{c} 1.16 \\ 0.066 \\ 1.44 \pm 0.04 \\ 0.72 \pm 0.02 \\ 0.21 \\ 0.35 \\ \end{array} \begin{array}{c} 1.13 \\ 3.72 \\ 3.71 \\ 3.72 \\ 0.37 \\ 0.37 \\ \end{array} \begin{array}{c} 0.066 \\ 0.14 \\ 3.41 \pm 0.08 \\ 1.70 \pm 0.04 \\ 0.83 \pm 0.02 \\ 0.02 \\ 0.48 \pm 0.01 \\ 1.14 \pm 0.03 \\ \end{array} \begin{array}{c} 0.35 \\ 0.28 \\ 0.62 \\ 0.16 \\ 3.62 \\ 13.00 \\ 0.28 \\ 7.19 \pm 0.15 \\ 3.59 \pm 0.08 \\ 12.55 \pm 0.27 \\ 8.37 \pm 0.18 \\ \end{array} \begin{array}{c} 0.02 \\ 0.28 \\ 0.68 \\ 25.10 \pm 0.53 \\ 12.55 \pm 0.27 \\ 8.37 \pm 0.18 \\ 0.18 \\ 0.11 \\ 0.11 \\ 0.11 \\ 0.12 \\ 0.$	W1	0.02	20.2	3.7	2.25	0.051	$1.22 \pm 0.03$	$0.61 \pm 0.01$	$0.41 \pm 0.01$
$\begin{array}{c} \text{W1} & 0.52 \\ \text{W1} & 0.64 \\ \text{W1} & 0.64 \\ \text{W1} & 1.16 \\ \text{UP} & 1.18 \\ \text{UP} & 1.13 \\ \text{UP} & 1.18 \\ \text{UP} & 1.13 \\ \text{UP} & 1.13 \\ \text{UP} & 1.13 \\ \text{UP} & 1.14 \\$	W1	0.14	10.9	3.73	4.72	0.10	$2.53 \pm 0.06$	$1.27\pm0.03$	$0.84 \pm 0.02$
$\begin{array}{cccccccccccccccccccccccccccccccccccc$	W1	0.26	11.13	3.73	4.45	0.10	$2.39 \pm 0.06$	$1.19 \pm 0.03$	$0.80 \pm 0.02$
$\begin{array}{c} \text{W1} & 1.16 \\ \text{W1} & 1.27 \\ \text{H68.23} & 3.29 \\ \text{W2} & 27.80 \\ \text{W3} & 0.59 \\ \text{H6.91} \pm 0.36 \\ \text{W3} & 25.99 \pm 0.28 \\ \text{W3} & 1.61 \\ \text{H7.06} & 3.21 \\ \text{W2} & 0.07 \\ \text{H7.82} & 3.71 \\ \text{W3} & 3.09 \\ \text{W2} & 0.07 \\ \text{W2} & 0.21 \\ \text{H8.17} & 3.71 \\ \text{W3} & 2.67 \\ \text{W3} & 0.066 \\ \text{W2} & 0.35 \\ \text{H3.87} & 3.72 \\ \text{H3.87} & 3.72 \\ \text{H3.13} & 3.72 \\ \text{H4.63} & 0.89 \\ \text{H4.21} & 3.72 \\ \text{H5.20} & 0.066 \\ \text{H4.4} \pm 0.04 \\ \text{H5.10} & 0.72 \pm 0.02 \\ \text{H5.10} & 0.05 \\ \text{H5.10} & 0.083 \pm 0.02 \\ \text{H5.10} & 0.56 \pm 0.01 \\ \text{H5.10} & 0.066 \\ \text{H5.10} & 0.083 \pm 0.02 \\ \text{H5.10} & 0.056 \pm 0.01 \\ \text{H5.10} & 0.066 \\ \text{H5.10} & 0.083 \pm 0.02 \\ \text{H5.10} & 0.056 \pm 0.01 \\ \text{H5.10} & 0.04 \\ \text{H5.10} & 0.083 \pm 0.02 \\ \text{H5.10} & 0.056 \pm 0.01 \\ \text{H5.10} & 0.04 \\ \text{H5.10} & 0.04$	W1	0.52	30.34	3.67	3.62	0.073	$1.97 \pm 0.04$	$0.98 \pm 0.02$	$0.66 \pm 0.01$
$\begin{array}{cccccccccccccccccccccccccccccccccccc$	W1	0.64	18.84	3.71	3.27	0.081	$1.76 \pm 0.04$	$0.88 \pm 0.02$	$0.59 \pm 0.01$
$\begin{array}{cccccccccccccccccccccccccccccccccccc$	W1	1.16	19.83	3.7	26.90	0.57	$14.53 \pm 0.31$	$7.26 \pm 0.15$	$4.84 \pm 0.10$
$\begin{array}{cccccccccccccccccccccccccccccccccccc$	W1	1.27	168.23	3.29	27.80	0.59	$16.91 \pm 0.36$	$8.46 \pm 0.18$	$5.64 \pm 0.12$
$\begin{array}{cccccccccccccccccccccccccccccccccccc$	W1	1.61	197.06	3.21	41.68	0.89	$25.99 \pm 0.55$	$12.99 \pm 0.28$	$8.66 \pm 0.18$
$\begin{array}{cccccccccccccccccccccccccccccccccccc$	W2	0.07	17.82	3.71	3.09	0.073	$1.67 \pm 0.04$	$0.83 \pm 0.02$	$0.56 \pm 0.01$
$\begin{array}{cccccccccccccccccccccccccccccccccccc$	W2	0.21	18.17	3.71	2.67	0.066	$1.44 \pm 0.04$	$0.72 \pm 0.02$	$0.48 \pm 0.01$
$\begin{array}{cccccccccccccccccccccccccccccccccccc$	W2	0.35	13.87	3.72	6.34	0.14	$3.41 \pm 0.08$	$1.70 \pm 0.04$	$1.14 \pm 0.03$
$\begin{array}{cccccccccccccccccccccccccccccccccccc$	W2	0.48	14.21	3.72	8.79	0.19	$4.72 \pm 0.10$	$2.36 \pm 0.05$	$1.58 \pm 0.03$
$\begin{array}{cccccccccccccccccccccccccccccccccccc$	W2	0.62	50.16	3.62	13.00	0.28	$7.19 \pm 0.15$	$3.59 \pm 0.08$	$2.40 \pm 0.05$
$\begin{array}{cccccccccccccccccccccccccccccccccccc$	W2	1.13	426.46	2.56	32.19	0.68	$25.10 \pm 0.53$	$12.55 \pm 0.27$	$8.37 \pm 0.18$
$\begin{array}{cccccccccccccccccccccccccccccccccccc$	W2	1.25	348.86	2.78	32.39	0.69	$23.29 \pm 0.50$	$11.64 \pm 0.25$	$7.76 \pm 0.17$
$\begin{array}{cccccccccccccccccccccccccccccccccccc$	W3	1.1	112.28	3.44	73.20	1.56	$42.50 \pm 0.90$	$21.25 \pm 0.45$	$14.17 \pm 0.30$
$\begin{array}{cccccccccccccccccccccccccccccccccccc$	W4	0.67	24.7	3.69	36.77	0.79	$19.93 \pm 0.43$	$9.97 \pm 0.21$	$6.64 \pm 0.14$
$\begin{array}{cccccccccccccccccccccccccccccccccccc$	S1	0.14	52.87	3.61	17.57	0.37	$9.73 \pm 0.21$	$4.87 \pm 0.10$	$3.24 \pm 0.07$
$\begin{array}{cccccccccccccccccccccccccccccccccccc$	S4	0.51	52.66	3.61	13.92	0.31	$7.71 \pm 0.17$	$3.85 \pm 0.09$	$2.57 \pm 0.06$
$\begin{array}{cccccccccccccccccccccccccccccccccccc$	S4	1.27	10.45	3.73	12.95	0.27	$6.95 \pm 0.15$	$3.47 \pm 0.07$	$2.32 \pm 0.05$
$\begin{array}{cccccccccccccccccccccccccccccccccccc$	S5	0.06	25.22	3.69	10.16	0.23	$5.51 \pm 0.12$	$2.75 \pm 0.06$	$1.84 \pm 0.04$
$\begin{array}{cccccccccccccccccccccccccccccccccccc$	S5	0.18	34.96	3.66	2.52	0.051	$1.38 \pm 0.03$	$0.69 \pm 0.01$	$0.46 \pm 0.01$
85 $0.53$ $51.68$ $3.61$ $8.28$ $0.18$ $4.58 \pm 0.10$ $2.29 \pm 0.05$ $1.53 \pm 0.03$ 85 $0.65$ $37.45$ $3.65$ $12.89$ $0.28$ $7.06 \pm 0.15$ $3.53 \pm 0.08$ $2.35 \pm 0.05$ 85 $0.77$ $111.78$ $3.45$ $13.36$ $0.28$ $7.76 \pm 0.16$ $3.88 \pm 0.08$ $2.59 \pm 0.05$ 85 $0.88$ $66.13$ $3.55$ $12.69$ $0.27$ $7.14 \pm 0.15$ $3.57 \pm 0.08$ $2.38 \pm 0.05$ 85 $1.05$ $12.98$ $3.72$ $12.69$ $0.27$ $6.82 \pm 0.15$ $3.41 \pm 0.07$ $2.27 \pm 0.05$ 85 $1.16$ $481.26$ $2.41$ $9.68$ $0.21$ $8.03 \pm 0.17$ $4.01 \pm 0.09$ $2.68 \pm 0.06$	S5	0.3	24.6	3.69	2.90	0.066	$1.57 \pm 0.04$	$0.79 \pm 0.02$	$0.53 \pm 0.01$
$\begin{array}{cccccccccccccccccccccccccccccccccccc$	S5	0.41	29.92	3.68	5.18	0.12	$2.82 \pm 0.06$	$1.41 \pm 0.03$	$0.94 \pm 0.02$
85       0.77       111.78       3.45       13.36       0.28 $7.76 \pm 0.16$ $3.88 \pm 0.08$ $2.59 \pm 0.05$ 85       0.88       66.13       3.55       12.69       0.27 $7.14 \pm 0.15$ $3.57 \pm 0.08$ $2.38 \pm 0.05$ 85       1.05       12.98       3.72       12.69       0.27 $6.82 \pm 0.15$ $3.41 \pm 0.07$ $2.27 \pm 0.05$ 85       1.16       481.26       2.41       9.68       0.21 $8.03 \pm 0.17$ $4.01 \pm 0.09$ $2.68 \pm 0.06$	S5	0.53	51.68	3.61	8.28	0.18	$4.58 \pm 0.10$	$2.29 \pm 0.05$	$1.53 \pm 0.03$
S5 $0.88$ $66.13$ $3.55$ $12.69$ $0.27$ $7.14 \pm 0.15$ $3.57 \pm 0.08$ $2.38 \pm 0.05$ S5 $1.05$ $12.98$ $3.72$ $12.69$ $0.27$ $6.82 \pm 0.15$ $3.41 \pm 0.07$ $2.27 \pm 0.05$ S5 $1.16$ $481.26$ $2.41$ $9.68$ $0.21$ $8.03 \pm 0.17$ $4.01 \pm 0.09$ $2.68 \pm 0.06$	S5	0.65	37.45	3.65	12.89	0.28	$7.06 \pm 0.15$	$3.53 \pm 0.08$	$2.35 \pm 0.05$
85       1.05       12.98       3.72       12.69       0.27 $6.82 \pm 0.15$ $3.41 \pm 0.07$ $2.27 \pm 0.05$ 85       1.16       481.26       2.41       9.68       0.21 $8.03 \pm 0.17$ $4.01 \pm 0.09$ $2.68 \pm 0.06$	S5	0.77	111.78	3.45	13.36	0.28	$7.76 \pm 0.16$	$3.88 \pm 0.08$	$2.59 \pm 0.05$
S5 1.16 481.26 2.41 9.68 0.21 $8.03 \pm 0.17$ $4.01 \pm 0.09$ $2.68 \pm 0.06$	S5	0.88	66.13	3.55	12.69	0.27	$7.14 \pm 0.15$	$3.57 \pm 0.08$	$2.38 \pm 0.05$
	S5	1.05	12.98	3.72	12.69	0.27	$6.82 \pm 0.15$	$3.41 \pm 0.07$	$2.27 \pm 0.05$
S5 1.28 497.53 2.37 11.50 0.24 $9.72 \pm 0.21$ $4.86 \pm 0.10$ $3.24 \pm 0.07$	S5	1.16	481.26	2.41	9.68	0.21	$8.03 \pm 0.17$	$4.01 \pm 0.09$	$2.68 \pm 0.06$
	S5	1.28	497.53	2.37	11.50	0.24	$9.72 \pm 0.21$	$4.86 \pm 0.10$	$3.24 \pm 0.07$

S5 1.64 237.92 3.09 40.16 0.86  $25.97 \pm 0.56$   $12.98 \pm 0.28$   $8.66 \pm 0.19$ 

# S3. Sediment cores

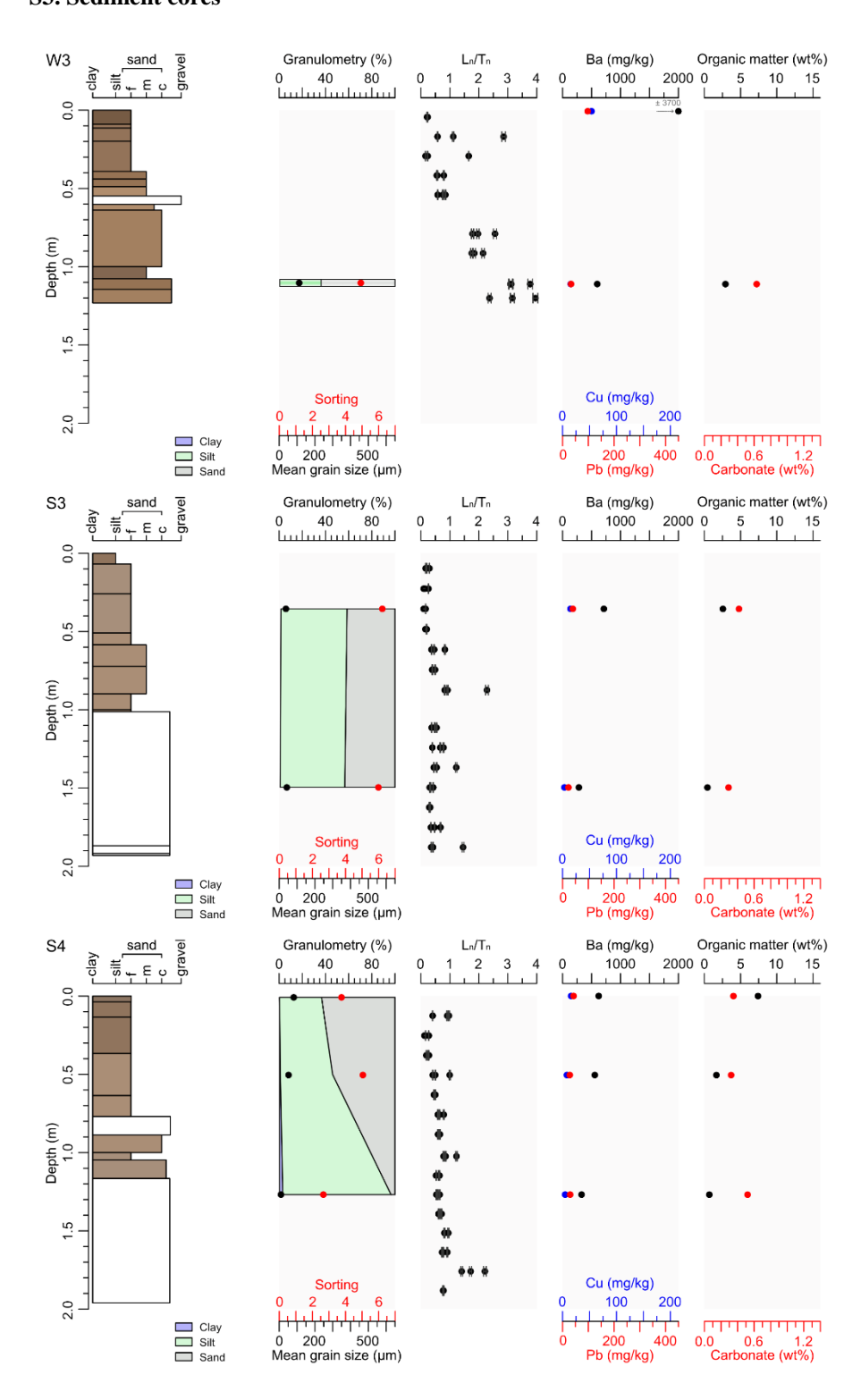


Figure S3. Stratigraphic logs of the W3 (Wolfach), S3, and S4 (Schenkenzell) cores including horizons shown in Munsell colours. The columns display (from left to right): grain-size distributions,  $L_n/T_n$  values (black), concentration of Ba (black), Pb (red), and Cu (blue), and the wt% of both organic matter and carbonate.

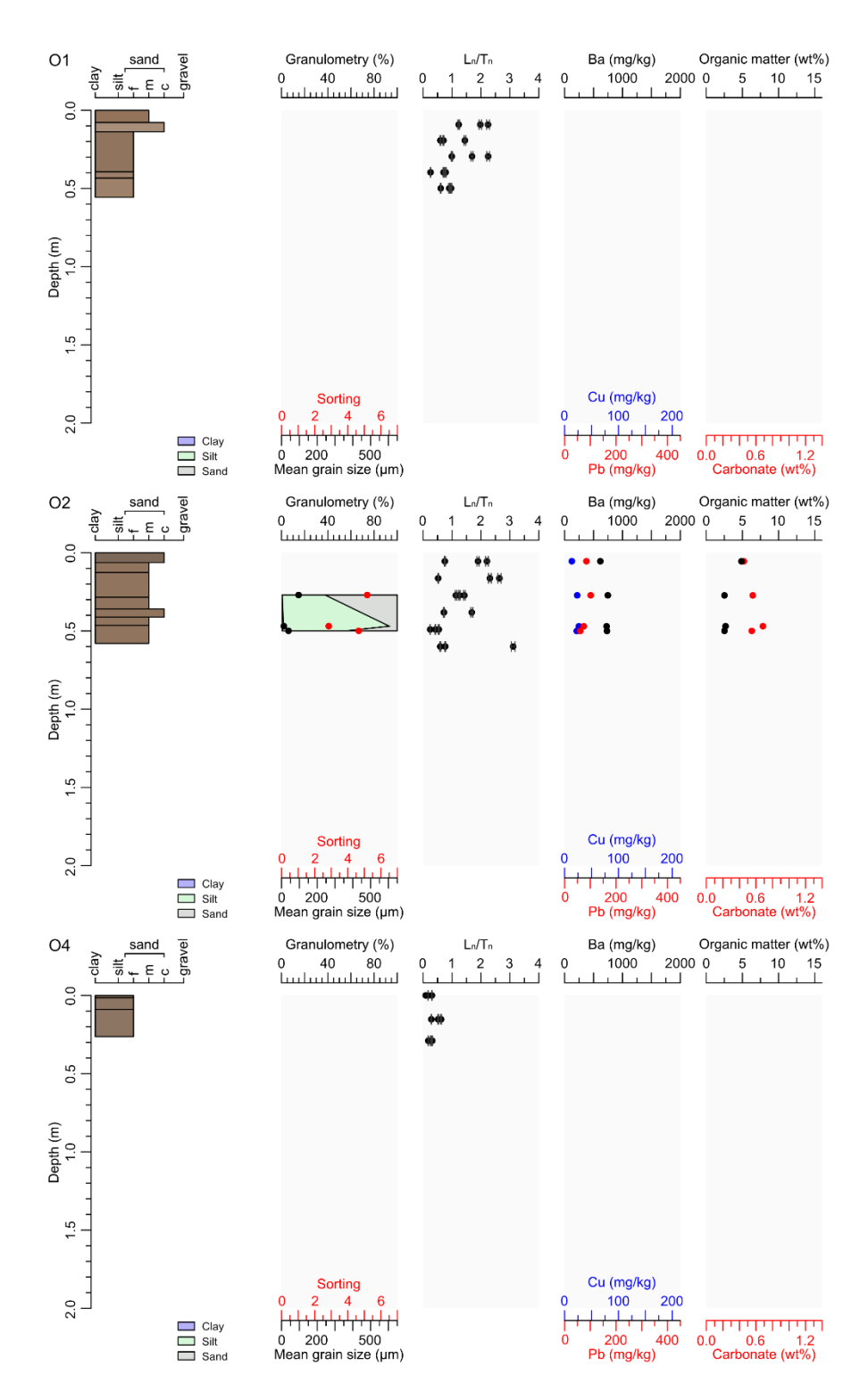


Figure S4. Stratigraphic logs of the O1, O2, and O4 (Oberwolfach) cores including horizons shown in Munsell colours. The columns display (from left to right): grain-size distributions,  $L_n/T_n$  values (black), concentration of Ba (black), Pb (red), and Cu (blue), and the wt% of both organic matter and carbonate.

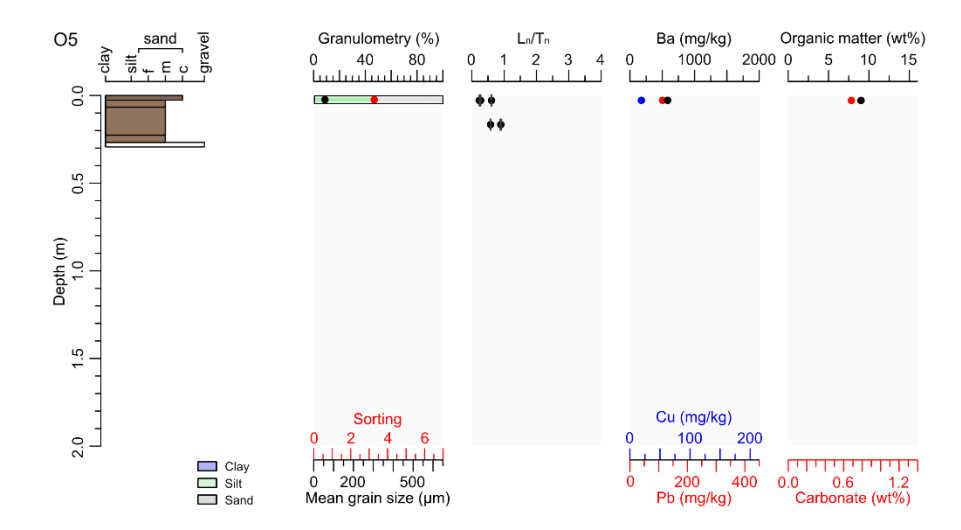


Figure S5. Stratigraphic logs of the O5 (Oberwolfach) core including horizons shown in Munsell colours. The columns display (from left to right): grain-size distributions,  $L_n/T_n$  values (black), concentration of Ba (black), Pb (red), and Cu (blue), and the wt% of both organic matter and carbonate.

# S4. Heavy metal analyses

Concerning the geochemical analysis, the concentration-depth models of the sediment cores were studied by the fit of linear or logatirhmic models and the data set association between the pXRF and EDX by correlation coefficients. Generally speaking, best concentration-depth fits for all data points per core were logarithmic models, which holds for both the pXRF and EDX data (exceptions, i.e. models with too similar R<sup>2</sup> values, in Table 10). In comparison, fitting models to all data points per element, considering the unreliable data (Table 10), did not find a generally preferred model type for the pXRF data, whereas logarithmic models fitted the EDX data best. Then, the data set association tests found that almost all core-element combinations had positive coefficients, meaning the increase or decrease of the element in a profile was in similar direction for both datasets. Additionally, the absolute values were generally high even though the range in number of data points was large. Hence, the element-depth slopes for the EDX data, derived after the normalisation-step, are similar, yet should not be interpreted individually due to the small sample sizes.

# S4.1. Geochemical analysis: pXRF

Before measuring a new core, the in-house standard CS-M2 provided by Bruker was measured ten times to ensure precision and accuracy. Measurements of the in-house standard CS-M2 revealed mean Al<sub>2</sub>O<sub>3</sub>, K<sub>2</sub>O, Ca, Mn, Fe, Cu, and Pb concentrations within the minimum and maximum acceptance limits of Bruker. All measurements (standard and samples) were conducted in the GeoExploration mode lasting three times 20 s. Measurements with count-rates below internal thresholds were rejected. After each measurement, the detection window of the analyser was cleaned.

### S4.2. Geochemical analysis: EDX sample preparation and measurement

Sample preparation for the EDX measurements included air-drying, sieving to < 2 mm (including root and wood fragment extraction) and homogenisation to a flour-like consistency using a mortar and pestle before measurement.

The measurement was done using an Epsilon 4 instrument (PANalytical). The bulk powder samples were filled into spectro cups and sealed with a Mylar film of six mm thickness. A silver X-ray tube was used as radiation source. The tube conditions (5-50kv, 600 W, 2-60 mA) were adapted depending on the element and respective filter (Ti, Al-50, Al-200, Ag, Cu-500). Most of the major elements (Al<sub>2</sub>O<sub>3</sub>, MgO, SiO<sub>2</sub>, Na<sub>2</sub>O) were measured in a He atmosphere. A silicon rift detector was used for detection and quantification. The calibration is based on numerous different international certified soil and rock standards. The accuracy was checked by including four reference materials (GXR2, GXR5, GXR6, and AGV-1; Govindaraju (1994)) into the measurement protocol (accuracy average  $\pm$  1.1 %,  $\pm$  1.4 %,  $\pm$  0.6 %, and  $\pm$  1.2 % for elements in Table 10 and V).

# S4.3. Geochemical analysis: statistical comparisons pXRF and EDX

Data processing of the coefficient of determination ( $R^2$ ) of linear and logarithmic concentration-depth models included further categorisation. This was based on the absolute difference between the model  $R^2$ s if both model fits were possible, only when there was a min. |1 %| difference. Model fits were only partially successful as indicated by the large spread in  $R^2$  values (Table S7).

Data preprocessing for computing the Pearson (r) and Spearman's rank correlation coefficients consisted of normalising values between 0-1 and ranking. Additionally, it included omitting MnO and Na<sub>2</sub>O due to incompleteness in the dataset, low EDX measurement quality for Na<sub>2</sub>O, and reduced number of both data points (from 73 to 69) and r to -0.82 when including these.

# S4.4. Geochemical analysis: reference element enrichment factors

Reference element suitability for enrichment factors, like discussed by Álvarez-Vázquez et al. (2020), was assessed with regression modelling of elements (judged by R<sup>2</sup>) with the MZ, considering EDX data quality (accuracy indicators Table S7). Vanadium (V) was found most suitable (Table S4, S5), having relatively stable concentrations in the datasets and just mainly atmospheric carbon dioxide (CO<sub>2</sub>) and ammonium (NH<sub>3</sub><sup>+</sup>) enhancing V leaching from soils (Mandiwana and Panichev, 2009). Heavy metal mobility needs to be considered as leaching likely enriches the horizons underlying the originally enriched layer. The mobility depends on, among others, soil pH, redox potential, and the presence of organic soil compounds (e.g. Oyewo et al., 2020; Kicińska et al., 2022).

# S4.5. Principal component analysis (PCA)

Studying linear correlations supported investigating whether the heavy element trends are predictable by core depth, grain-size, loss-on-ignition (LOI) outcomes, IRSL screening (L<sub>n</sub>/T<sub>n</sub>), or major element oxides. Since some of these properties are composed of several individual variables, a principal component analysis (PCA) was performed. A PCA represents data in smaller sets of variables, namely a low-dimensional subset of the parameter space, maintaining the strongest variations among the samples. The respective properties (heavy metal content, grain-size, LOI, and major element oxide concentration) were represented by their first principal component (PC). Correlations between individual variables (here the variable that contributes most to the first PC) and the first PC of the heavy element were investigated to study if PCs yield higher correlations than the individual variables. The PCA applied inverse variance weighting, equivalent to normalising the original variables to unit variance. In addition, natural logarithms of mean grain-sizes and sorting coefficients were used.

Whether heavy element trends, i.e. first PC, are predictable by other core characteristics, the strongest linear correlation exists between the first PCs of the LOI (r = 0.85) and the major element oxides (r = -0.86) (Fig. S6, Table S8, other properties: Fig. S8, Fig. S9). These trend lines ( $R^2 = r^2 \approx 0.73$ ) indicate that 73 % of the first PC of the elements variance can be explained by the first PC of either the LOI or the major element oxides by linear regression. However, as shown in Fig. S6 (left), the Wolfach data dominates the LOI correlation, shown by the range covered, and the Oberwolfach data shows a slight opposite trend relative to the overall trend line. Contrastingly, all major element oxide trends (Fig. S6 right) fit the overall trend line and range better. Despite the similar overall correlation, it suggests the major element oxides to be a better predictor for the heavy elements than the LOI. However, the two properties are not independent (Fig. S7) even though their combined correlation (r = -0.76) is weaker than the respective correlations with the heavy elements. Additionally, the LOI data contains the structural water component, making the PC interpretation more complex. Hence, combining these first PCs into an improved predictor for the elements would bear the risk of overparameterisation. Apart from these PCs, r values with the other core characteristics were low of which interpretations are problematic due to the complex dependencies of these characteristics on other factors that are not explicitly considered in the analysis (Table S8, Fig. S6, Fig. S7).

Interpretation of the correlation coefficients of the PCA was done carefully. Namely, the computations follow the assumption of linearity between two correlated properties, meaning low coefficients point to either a weak correlation or an underestimation due to non-linearity. Additionally, varying data set sizes per study site skew the data interpretation. Curiously, considering both the LOI 550 °C and 950 °C as predictors explains more variance in the heavy elements than those separately. Even though higher OM contents are positively correlated to heavy element concentrations, the high correlation coefficient for LOI 550 °C and 950 °C could be a coincidence (i.e., another process resulting in higher carbonate amounts simultaneous

with enhanced heavy element addition, a computational artefact) as this mechanism does not hold for carbonates. Additionally, the broken trend of increasing LOI and decreasing heavy element concentrations in Oberwolfach (left Fig. S6) cannot be the result of a changed chemical process of heavy metal-OM adsorption in recently deposited overbank fines. Finally, testing the two best properties together (Fig. S7) revealed that these do not carry fully independent information (r = -0.76). Thus, the LOI and major element oxides trends independently explain a large fraction of the heavy element variability, yet cannot explain all.

 $Table~S4.~Assessment~reference~element~by~linear~regression~between~element~concentrations~and~M_{Z},~based~on~unfavourable~EDX~measurement~quality~(EDX~unfit),~and~known~anthropogenic~influences~(Weber~and~Lehmkuhl,~2024).$ 

Element	W1 R <sup>2</sup>	W2 R <sup>2</sup>	S5 R <sup>2</sup>	Weighted average	EDX unfit	Anthropogenically influenced	Reference element suitability
As	0.7502	0.7836	0.045	0.5244		Applicable	-
Ba	0.3374	0.6551	0.0506	0.3301			Applicable
Cr	0.3791	0.6401	0.0204	0.3320	Applicable		
Cs	0.2481	0.6005	0.0069	0.2656	Applicable		
Cu	0.2989	0.6536	0.1484	0.3473			Applicable
Ga	0.4162	0.5953	0.0011	0.3276			Applicable
Mo	-	-	-	-	Applicable		
Nb	0.4425	0.6578	0.0696	0.3780			Applicable
Ni	0.3498	0.689	0.2774	0.4199		Applicable	
Pb	0.2464	0.5434	0.1006	0.2803		Applicable	
Rb	0.3036	0.6861	0.0001	0.3087			Applicable
S	0.1292	0.1186	0.0499	0.0998	Applicable		
Sb	-	-	-	-	Applicable	Applicable	
Sn	0.5961	0.0002	0.0311	0.2422	Applicable	Applicable	
Sr	0.2651	0.5685	0.1619	0.3150			Applicable
V	0.7382	0.4153	0.0812	0.4295			Applicable
Y	0.3161	0.4691	0.1814	0.3137			Applicable
Zn	0.2739	0.5334	0.1786	0.3142			Applicable
Zr	0.2756	0.8919	0.0742	0.3797		Applicable	
W	0.0283	0.0157	0.0003	0.0155	Applicable		
Th	0.1378	0.7165	0.033	0.2636	Applicable		
U	0.5657	0.6834	0.254	0.4945	Applicable		
Cd	-	-	-	-	Applicable		

Table S5. Enrichment factors (EFs) of heavy metal depth-trends determined with double normalisation on V. BG: background.

Type	Core	Depth (m bs)	As	Ba	Cu	Ga	Nb	Ni	Pb	Rb	Sr	Y	Zn	Zr
Value	W1	0.01	1.0	2.4	2.9	1.1	1.3	1.3	4.0	1.1	1.5	1.5	2.4	1.2
Value	W1	0.14	1.1	2.4	3.4	1.1	1.3	1.5	4.5	1.1	1.5	1.6	2.3	1.2
Value	W1	0.26	1.0	2.6	3.3	1.1	1.3	1.4	4.4	1.1	1.5	1.6	2.1	1.3
Value	W1	0.39	0.8	1.9	2.5	1.2	1.2	1.0	3.9	1.3	1.6	1.2	1.6	1.1
Value	W1	0.51	0.7	1.1	1.6	1.1	1.1	1.2	1.7	1.2	1.2	1.4	1.3	1.3
Value	W1	0.63	0.7	1.0	1.0	1.0	1.0	0.9	1.0	1.0	1.0	1.1	1.0	0.9
BG	W1	0.65	-	-	-	-	-	-	-	-	-	-	-	_
Value	W2	0.07	1.5	1.2	2.1	1.0	1.3	1.4	2.9	1.1	1.2	1.2	2.3	1.0
Value	W2	0.21	1.5	1.2	2.3	0.9	1.2	1.4	2.8	1.0	1.0	1.1	2.1	1.0
Value	W2	0.35	1.8	1.4	3.1	1.0	1.4	1.6	3.5	1.1	1.1	1.4	2.1	1.1
Value	W2	0.48	1.5	1.2	1.9	1.0	1.2	1.3	1.7	1.0	1.0	1.0	1.4	1.2
BG	W2	0.62	-	-	-	-	-	-	-	-	-	-	-	-
Value	S5	0.06	1.5	1.1	12.8	0.9	1.1	1.1	1.6	1.0	1.0	1.3	1.9	1.2
Value	S5	0.18	1.1	1.1	1.3	0.8	0.9	0.9	1.3	0.9	0.9	0.9	1.4	0.9
Value	S5	0.3	1.3	1.1	1.3	0.9	1.0	1.1	1.3	1.0	0.9	1.2	1.4	1.1
Value	S5	0.41	1.3	1.0	1.1	0.9	1.0	1.0	1.0	0.9	0.9	1.1	1.2	1.0
Value	S5	0.53	1.3	1.0	1.1	1.0	1.1	1.0	1.1	1.1	1.0	1.1	1.1	1.1
BG	S5	0.64	-	-	-	-	-	-	-	-	-	-	-	-

Table S6. Cores, number of datapoints per core, and Spearman's rank and Pearson correlation coefficients for the Ba, Pb, and Cu elements.

			Spearman	n's rank		Pearson		
Core	n_pXRF	n_EDX	Ba	Pb	Cu	Ba	Pb	Cu
W1	33	12	0.553	0.353	0.689	0.415	0.61	0.501
W2	26	10	0.539	0.583	0.689	0.698	0.55	0.442
W4	17	4	0.909	0.729	0.729	0.985	0.987	0.969
<b>S</b> 1	15	5	-0.463	0.706	0.706	0	-0.336	-0.227
S4	31	3	0.792	0.866	0.866	0.319	0.927	0.718
S5	32	13	0.186	0.407	0.407	-0.156	0.236	-0.002
S6	25	6	0.288	-0.405	-0.405	-0.141	0.359	-0.121

Table S7. Measurement method, data category (core, element), subject (core ID, element), R2 values of model types (logarithmic  $(R^2_{log})$ , linear  $(R^2_{lin})$  and their difference, including measurement quality indicators of not always accurate (\*), not accurate (\*\*), mainly below detection limit (\*\*\*).

Method	Category	Subject	$R^2_{log}$	$R^2_{lin}$	Higher R <sup>2</sup>	$R^2_{log}$ - $R^2_{lin}$ (%)
XRF	Core	W1	0.197	0.1942	Logarithmic	1.40%
XRF	Core	W2	0.3107	0.2589	Logarithmic	16.67%
XRF	Core	W3	0.1842	0.2278	Linear	-23.66%
XRF	Core	W4	0.2593	0.2769	Linear	-6.77%
XRF	Core	01	0.1608	0.1371	Logarithmic	14.73%
XRF	Core	O2	0.1975	0.1889	Logarithmic	4.35%
XRF	Core	O3	0.1357	0.1354	Logarithmic	0.25%
XRF	Core	O4	0.315	0.3161	Linear	-0.35%
XRF	Core	O5	0.3132	0.311	Logarithmic	0.72%
XRF	Core	S1	0.0955	0.0555	Logarithmic	41.96%
XRF	Core	S2	0.1343	0.09	Logarithmic	32.97%
XRF	Core	S3	0.4739	0.3121	Logarithmic	34.14%
XRF	Core	S4	0.1	0.1085	Linear	-8.44%
XRF	Core	S5	0.1441	0.1058	Logarithmic	26.57%
XRF	Core	S6	0.0319	0.0571	Linear	-79.19%
XRF	Element	$Al_2O_3$	0.1234	0.1107	Logarithmic	10.29%
XRF	Element	As	0.1117	0.3004	Linear	-168.85%
XRF	Element	Ba	0.3158	0.3016	Logarithmic	4.51%
XRF	Element	CaO				
XRF	Element	Cd		0.0318		
XRF	Element	Cr		0.0778		
XRF	Element	Cs				
XRF	Element	Cu	0.1125	0.2691	Linear	-139.19%
XRF	Element	$Fe_2O_3$				
XRF	Element	Ga	0.141	0.1455	Linear	-3.22%
XRF	Element	$K_2O$	0.094	0.089	Logarithmic	5.38%
XRF	Element	MgO	0.0496	0.0526	Linear	-6.00%
XRF	Element	MnO				
XRF	Element	Mo		0.0539		
XRF	Element	Na <sub>2</sub> O				
XRF	Element	Nb		0.1754		
XRF	Element	Ni	0.3527	0.2598	Logarithmic	26.33%
XRF	Element	$P_2O_5$				
XRF	Element	Pb	0.2355	0.322	Linear	-36.74%
XRF	Element	Rb	0.09	0.0898	Logarithmic	0.20%
XRF	Element	S	0.6613	0.3527	Logarithmic	46.66%
XRF	Element	Sb		0.0703		
XRF	Element	$SiO_2$	0.1206	0.1168	Logarithmic	3.15%
XRF	Element	Sn		0.0646		
XRF	Element	Sr	0.1773	0.16	Logarithmic	9.74%
XRF	Element	Th		0.0679		
XRF	Element	$TiO_2$				
XRF	Element	U		0.0841		

XRF	Element	V		0.1052		
XRF	Element	W		0.0564		
XRF	Element	Y	0.2572	0.272	Linear	-5.74%
XRF	Element	Zn	0.4266	0.4111	Logarithmic	3.63%
XRF	Element	Zr	0.3559	0.3875	Linear	-8.89%
EDX	Core	W1	0.683	0.6145	Logarithmic	10.03%
EDX	Core	W2	0.6789	0.6709	Logarithmic	1.18%
EDX	Core	W3				
EDX	Core	W4	0.7335	0.6798	Logarithmic	7.33%
EDX	Core	O1				
EDX	Core	O2	0.4705	0.4616	Logarithmic	1.90%
EDX	Core	O3				
EDX	Core	O4				
EDX	Core	O5				
EDX	Core	<b>S</b> 1	0.4633	0.4264	Logarithmic	7.98%
EDX	Core	S2	0.3345	0.2988	Logarithmic	10.69%
EDX	Core	S3				
EDX	Core	S4				
EDX	Core	S5	0.3979	0.4279	Linear	-7.56%
EDX	Core	S6	0.6047	0.6217	Linear	-2.81%
EDX	Element	$Al_2O_3*$	0.4786	0.4795	Linear	-0.18%
EDX	Element	As	0.6593	0.6773	Linear	-2.73%
EDX	Element	Ba	0.682	0.6586	Logarithmic	3.43%
EDX	Element	CaO	0.6536	0.6498	Logarithmic	0.57%
EDX	Element	Cd***	0.5081	0.3329	Logarithmic	34.48%
EDX	Element	Cr*	0.6103	0.4544	Logarithmic	25.54%
EDX	Element	Cs*	0.7402	0.6881	Logarithmic	7.05%
EDX	Element	Cu	0.5859	0.4798	Logarithmic	18.12%
EDX	Element	$Fe_2O_3$	0.6781	0.6993	Linear	-3.14%
EDX	Element	Ga	0.5939	0.5901	Logarithmic	0.65%
EDX	Element	$K_2O$	0.3808	0.3781	Logarithmic	0.70%
EDX	Element	MgO**	0.7112	0.7027	Logarithmic	1.18%
EDX	Element	MnO	0.7326	0.7234	Logarithmic	1.25%
EDX	Element	Mo***	0.2433	0.2216	Logarithmic	8.95%
EDX	Element	Na <sub>2</sub> O**	0.462	0.4959	Linear	-7.32%
EDX	Element	Nb	0.6108	0.6156	Linear	-0.79%
EDX	Element	Ni	0.5987	0.5817	Logarithmic	2.85%
EDX	Element	$P_2O_5**$	0.6977	0.6847	Logarithmic	1.85%
EDX	Element	Pb	0.6144	0.5589	Logarithmic	9.03%
EDX	Element	Rb	0.3716	0.3761	Linear	-1.22%
EDX	Element	S*	0.8691	0.8536	Logarithmic	1.78%
EDX	Element	Sb***		0.0815	-	
EDX	Element	$SiO_2$				
EDX	Element	Sn***	0.2092	0.4563	Linear	-118.11%
EDX	Element	Sr	0.2749	0.2751	Linear	-0.06%
EDX	Element	Th***	0.2067	0.1976	Logarithmic	4.40%
EDX	Element	$TiO_2$	0.7236	0.7234	Logarithmic	0.02%

EDX	Element	U***	0.2374	0.2292	Logarithmic	3.45%
EDX	Element	V	0.7431	0.7372	Logarithmic	0.80%
EDX	Element	W***	0.2997	0.2963	Logarithmic	1.14%
EDX	Element	Y	0.4843	0.4796	Logarithmic	0.98%
EDX	Element	Zn	0.6621	0.6175	Logarithmic	6.73%
EDX	Element	Zr	0.3875	0.3938	Linear	-1.62%

Table S8. Correlation coefficients with the first PC of the elements from the PCA analysis.

Property	Number of samples	Coefficient of correlation (r)
Depth (m)	73	-0.63
First PC loss on ignition	63	0.85
Loss on ignition 550 (%)	63	0.76
Loss on ignition 950 (%)	63	0.75
First PC grain-size	61	-0.53
$log10(M_z)$	61	-0.55
First PC element oxides	73	-0.86
$SiO_2$	73	-0.77

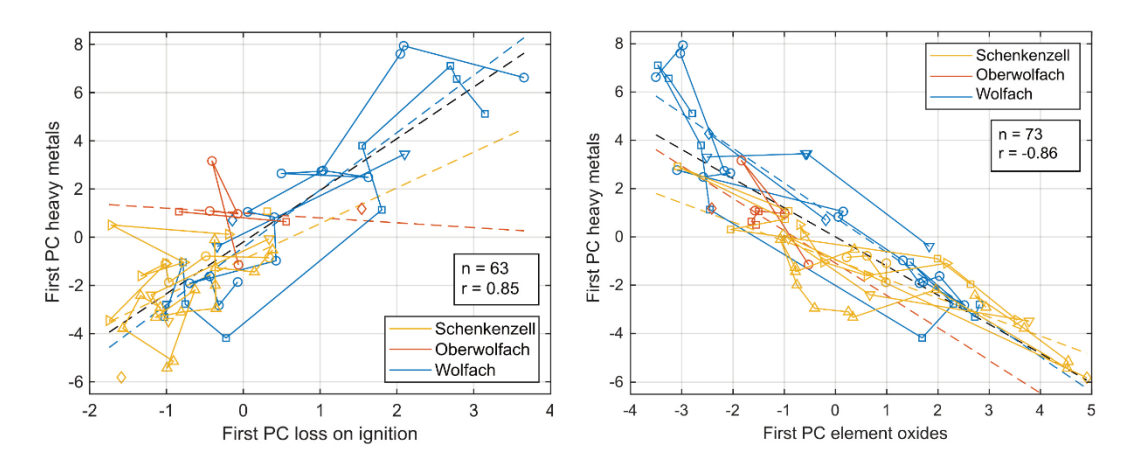


Figure S6. Left: PCA result on the LOI (combination of 550  $^{\circ}$ C and 950  $^{\circ}$ C) for the three study sites. Right: PCA result on the major element oxides (SiO<sub>2</sub>, Al<sub>2</sub>O<sub>3</sub>, Fe<sub>2</sub>O<sub>3</sub>, MgO, CaO, K<sub>2</sub>O, TiO<sub>2</sub>, P<sub>2</sub>O<sub>5</sub>) for the three study sites. Connecting lines indicate the individual cores. Dashed lines are trend lines for the individual sites (colour-coded to study sites) and for all sites together (black).

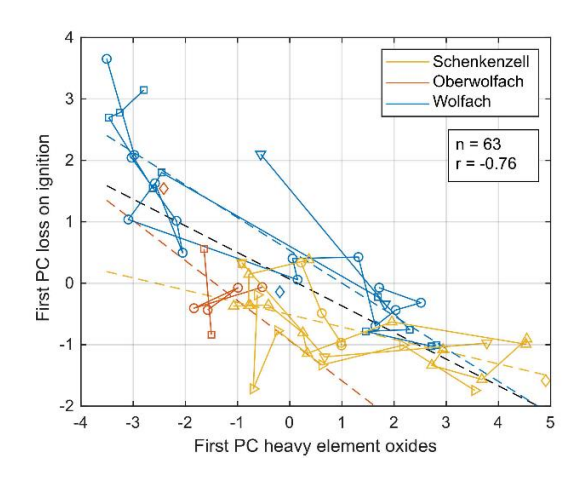


Figure S7. PCA result on the LOI (combination of 550  $^{\circ}$ C and 950  $^{\circ}$ C) and heavy element oxides (SiO<sub>2</sub>, Al<sub>2</sub>O<sub>3</sub>, Fe<sub>2</sub>O<sub>3</sub>, MgO, CaO, K<sub>2</sub>O, TiO<sub>2</sub>, P<sub>2</sub>O<sub>5</sub>) for the three study sites. Connecting lines indicate the individual cores. Dashed lines are trend lines for the individual sites (colour-coded to study sites)

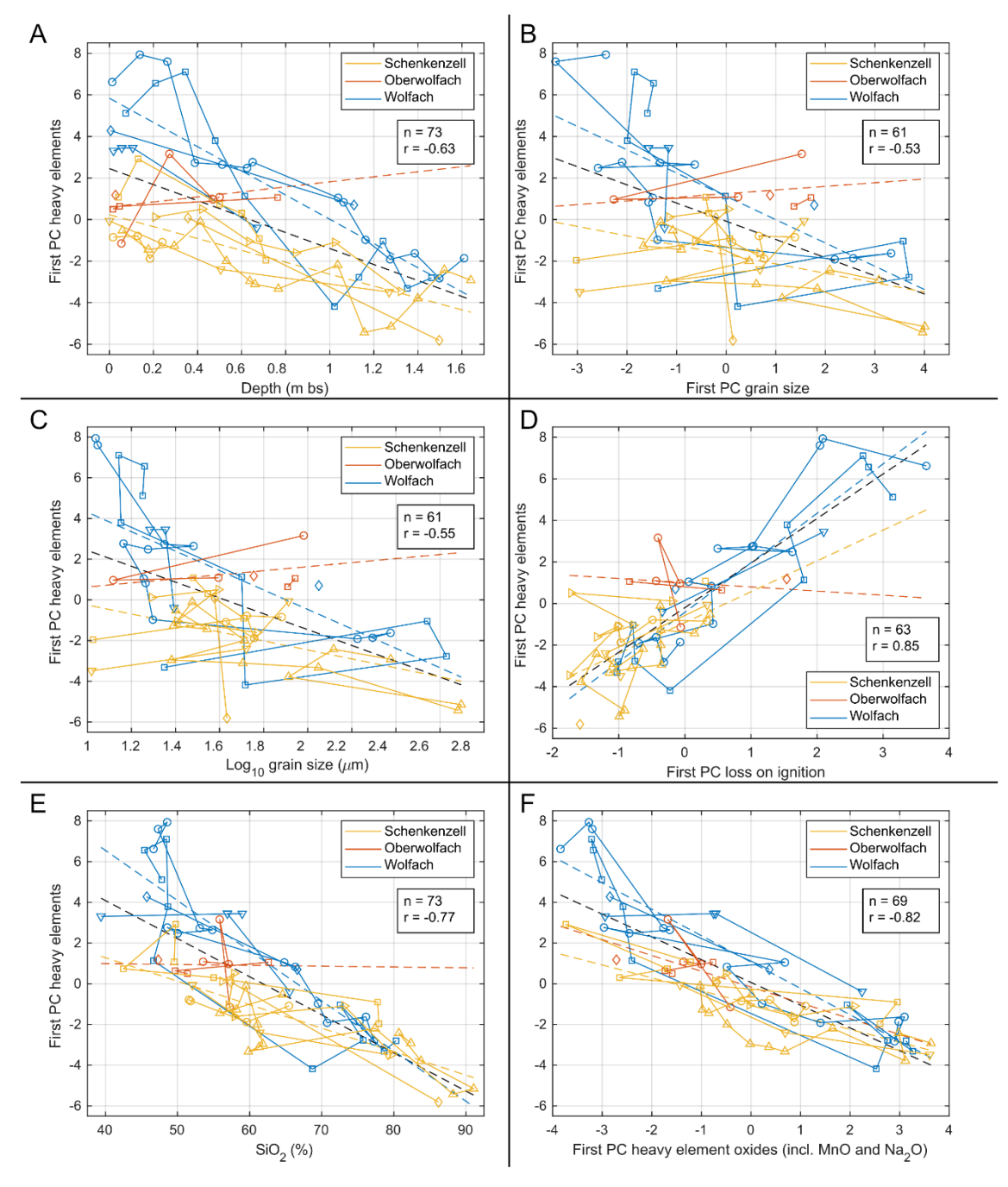


Figure S8. PCA result on the core depth (panel A), first PC grain-size (panel B),  $log_{10}(grain-size)$  (panel C), first PC LOI (panel D),  $SiO_2$  referred to as quartz (panel E), and first PC element oxides including MnO and  $Na_2O$  (panel F) versus the first PC heavy element for the three study sites. Connecting lines indicate the individual cores. Dashed lines are trend lines for the individual sites (colour-coded to study sites).

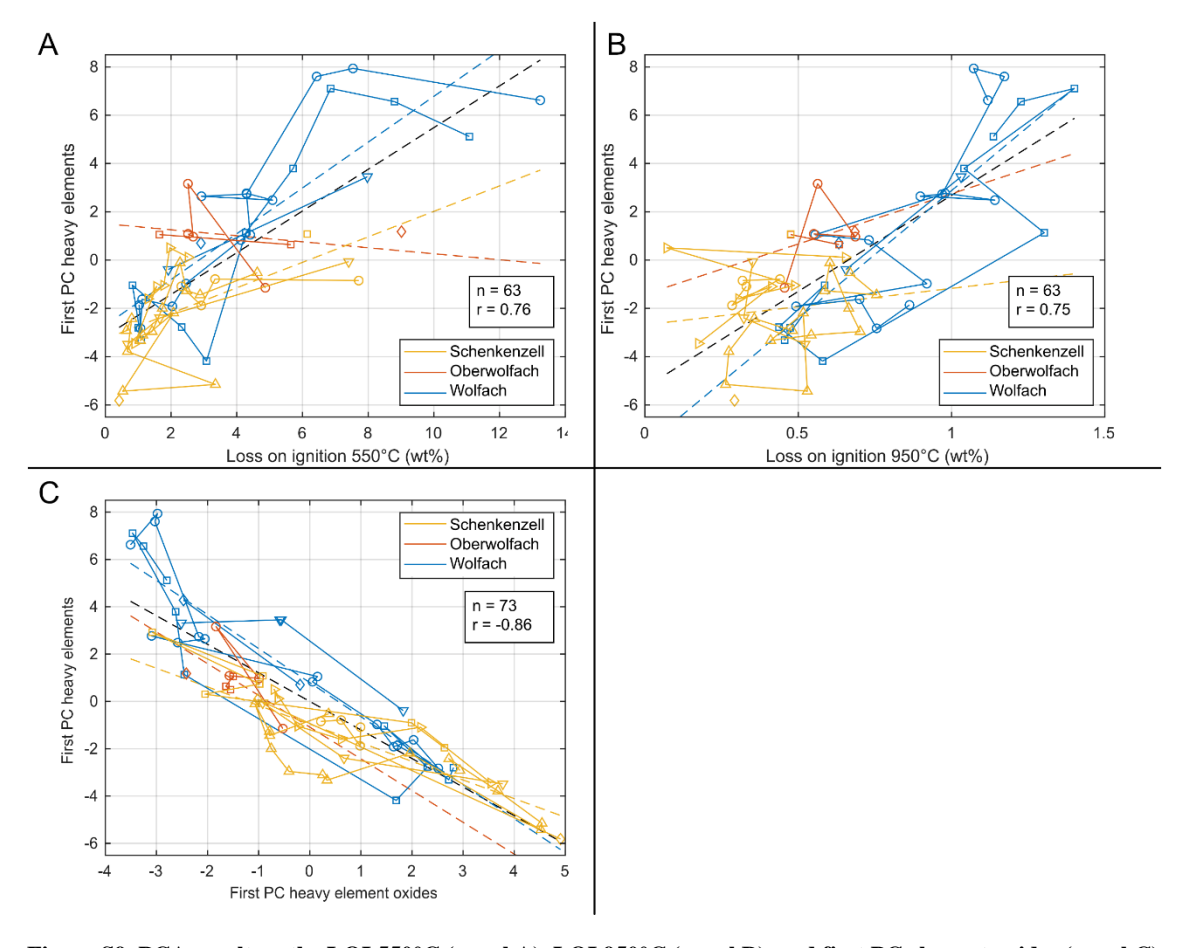


Figure S9. PCA result on the LOI  $550^{\circ}$ C (panel A), LOI  $950^{\circ}$ C (panel B), and first PC element oxides (panel C) versus the first PC heavy element for the three study sites. Connecting lines indicate the individual cores. Dashed lines are trend lines for the individual sites (colour-coded to study sites).

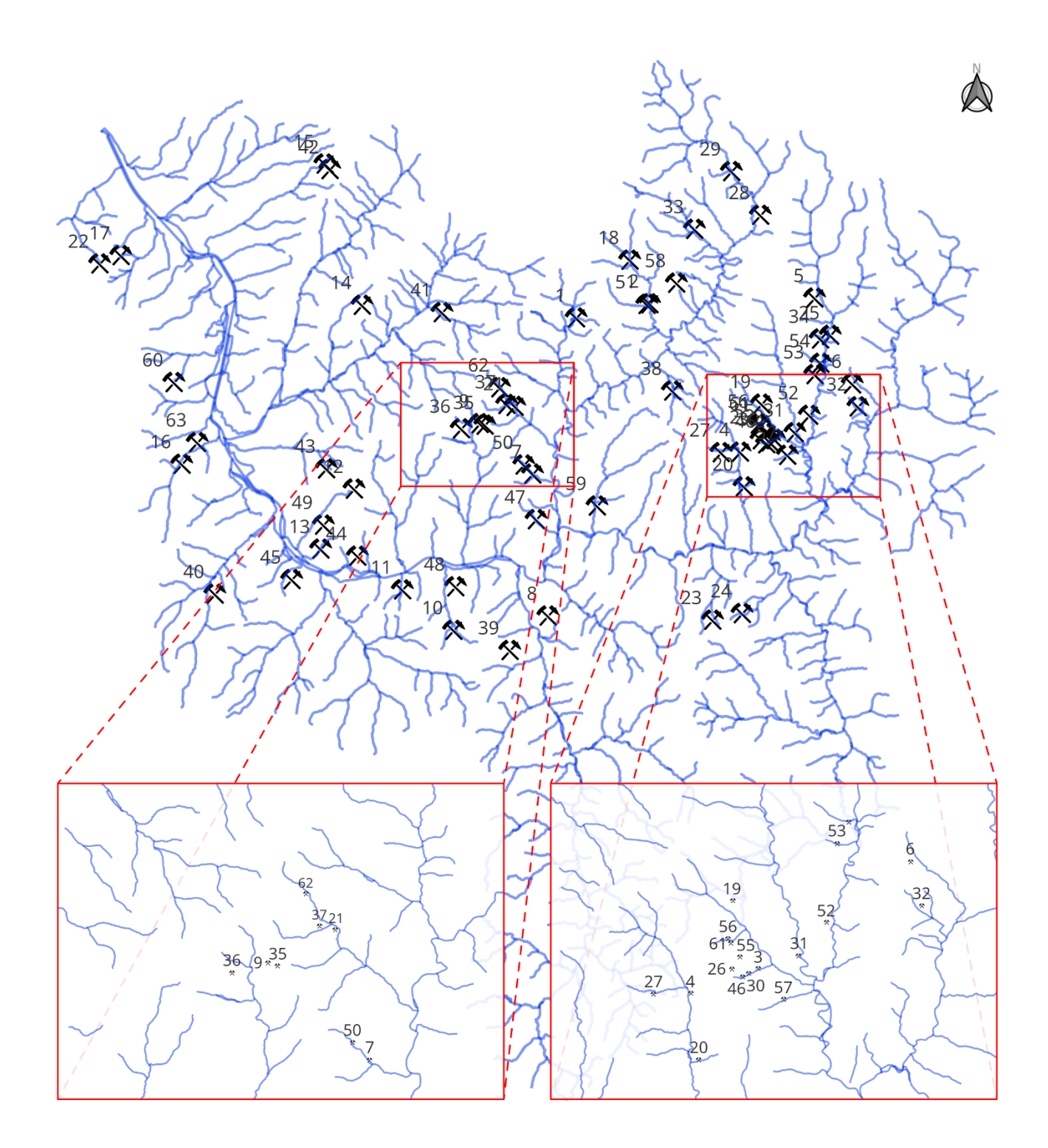


Figure S10. Map of mines in the Kinzig catchment (Table S8) including IDs with a focus on those along the main channel and northern tributaries. Sources: Mineralienatlas (https://www.mineralienatlas.de/) and Knausenberger (2001).

Table~S8.~List~of~mines~in~the~Kinzig~catchment~(Figure~S8)~including~IDs~with~a~focus~on~those~along~the~main~channel~and~northern~tributaries.~Sources:~Mineralienatlas~(https://www.mineralienatlas.de/)~and~Knausenberger~(2001).

ID	Mine	Mined	Ore vein
1	Grube Clara	Cu Ag Pb	Ba F
2	Grube Friedrich-Christian	Ag Co U	F
3	Grube Sophia	Ag Co	
4	Grube St. Anton	Co Ni Bi Ag U	
5	Grube Herzog Friedrich	Ag Co U	F
6	Grube Wolfgang und Eberhard	Ag Co Bi	Ba
7	Grube Wenzel	Ni Sb Ag	Ba
8	Grube Johannis Segen	Cu	Ba
9	Grube Erzengel Gabriel	Pb Ag	Ba F
10	Grube Bernhard	Ag Pb Zn	
11	Grube Ludwig	As Sb Pb Ag Au	
12	Grube Bergmanns trost	Ag	
13	Grube Segen Gottes	Pb Zn	
14	Grube Otto Schottenhöfe	Fe Cu Bi Mn	Ba
15	Grube Silberbrünnele	Cu Pb	Ba
16	Grube St. Mauritius		
17			
18	Grube Katharina		
19	Grube Güte Gottes	Co Ag	
20	Grube Katharina	Cu Co	
21	Grube Fortuna	Pb	Ba F
22		Coal	
23	Grube Hilfe Gottes	Cu Co Bi U	
24	Grube Johannes		
25	Grube Dreikönigstern	Ag Bi Co U	Ba F
26	Grube Simson	Ag Co	
27	Grube Katharina im Trillengrund	Cu Bi	Ba
28	Grube Daniel im Dehs	Cu	Ba
29	Grube Prosper	Cu	Ba
30	Grube Neuglück	Co	Ba
31	Grube Ilse		Ba F
32	Grube Gottes Segen	Pb Zn Ag	Ba F
33	Grube St. Georg	Cu	Ba
34	Grube Moses Segen	Ag Co Bi U	
35	Grube Maria Josepha	Ag Cu	
36	Grube Martin	Cu	Ba
37	Grube Ludwigs Trost	Pb Zn Ag	
38	Gruben St. Ferdinand und Josephs Treu	Cu	Ba
39	Grube Michelsberg	Cu	Ba
40	Grube Ursula	Sb Zn	
41	Grube Anna	Pb Ag	
42	Grube Amalie bzw. St. Jakob	Cu Ag	Ba
43	Grube Barbara	Ag	
44	Grube Anna	Pb Ag	
45	Grube Drey oder Treu Silberwerk	Pb Ag	Ba F

16	Grube Alt. St. Joseph	Ag Co	
47	Grube Dismas	Ba Fe Pb	
48	Grube Elisabeth	Fe	
49	Grube Maria Antoinette		
50	Grube Neuwenzel	Cu Co Ba	
51	Grube Emanuel Gottlieb		
52	Grube Alte Gabe Gottes		F
53	Grube Rafael	Cu Bi Ba	Ba F
54	Grube Hengstbach	Ag Co U	F
55	Grube Neu St. Joseph		
56	Grube David		
57	Grube König David		
58	Grube Gottes Gabe am Kupferberg	Cu	
59	Grube Ludwig	Ag Pb	
60	Grube St. Ferdinand	Cu	Ba
61	Grube Neu St. Ludwig		
62	Grube Herrenbusch		
63	Grube Marianne		Ba Cu

# S5. Historic maps

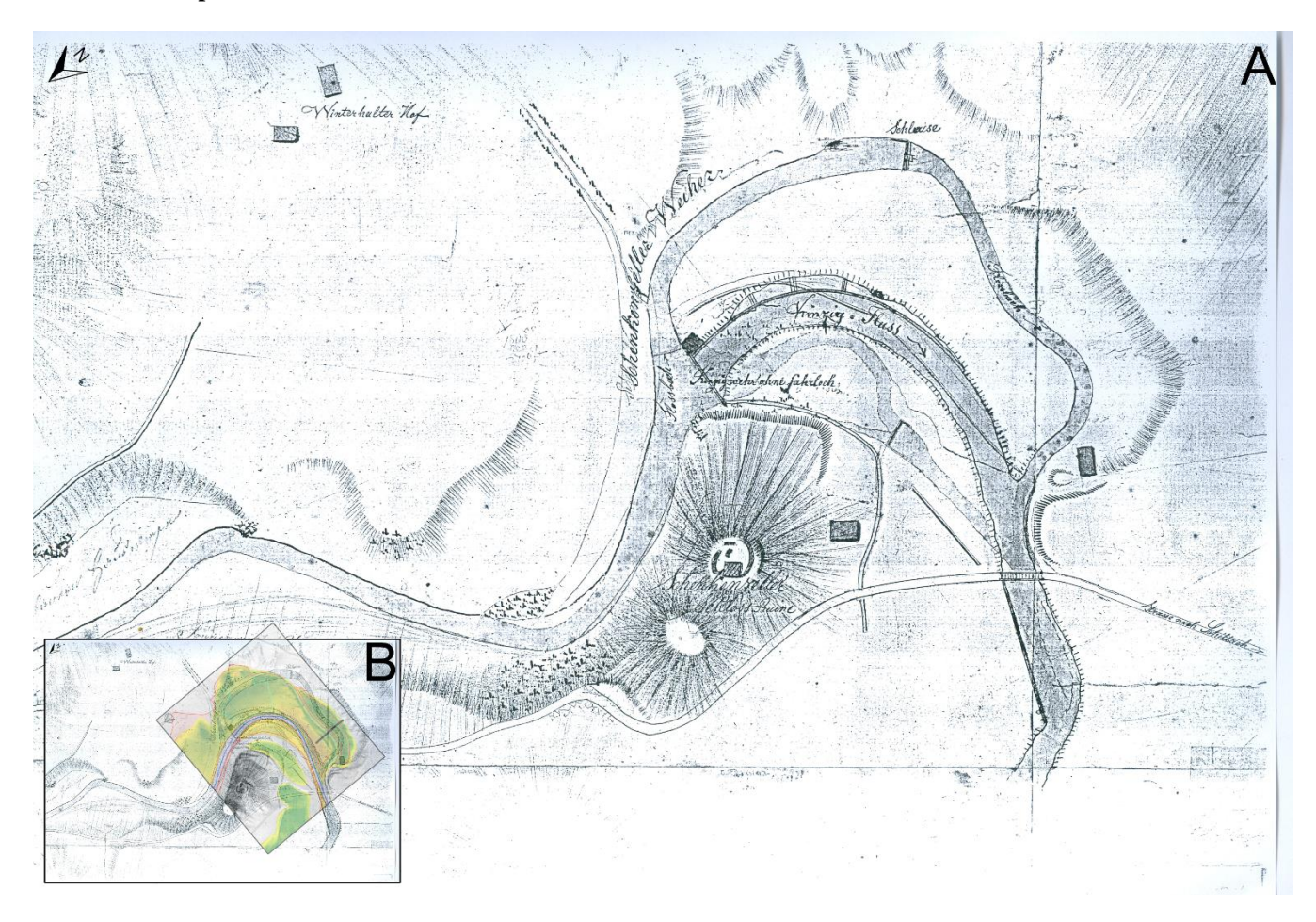


Figure S11. Panel A: historic map of the Schenkenzell study site from the year 1816, Stadtarchiv (city archive) Schiltach. Shown on the map are a wood slide (straight structure slightly left of the top middle, right of the "Winterhalter Hof") toward the Kinzig channel, the channel for timber drift and raft (top, "Flossbach"), weirs (divergence of main and timber channel by the "Schenkenzeller weiher", in the timber channel "Flossschleuse"), and binding site (likely between the main channel and channel for drift and raft). Panel B: overlay of study site as a reference to modern situation.



Figure S12. Panel A: historic map of the Schenkenzell study site from the year 1896, Stadtarchiv (city archive) Schiltach. Shown on the map are the Kinzig channel (potentially drawn in point bars in the curve on the left and just before the stream convergenace on the right) and the channel for timber drift and raft (right). Panel B: overlay of study site as a reference to modern situation.

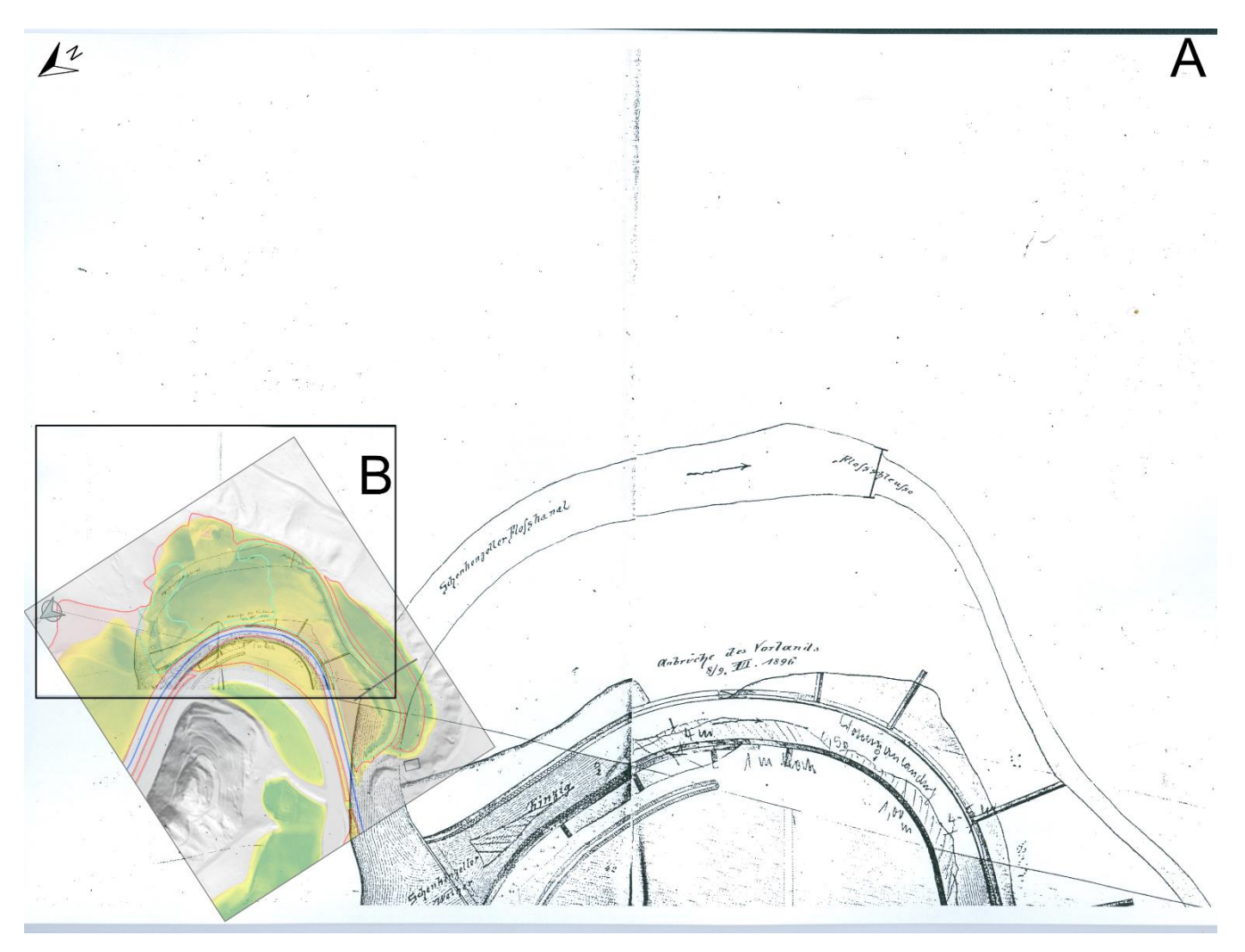


Figure S13. Panel A: historic map of the Schenkenzell study site from the year 1869, Stadtarchiv (city archive) Schiltach. Shown on the map are the Kinzig channel (potentially drawn in point bars in the middle of the bend, bottom side), the channel for timber drift and raft (top, "Schenkenzeller Flosskanal"), weirs (divergence of main and timber channel by the "Schenkenzeller weiher", in the timber channel "Flossschleuse"), binding site (likely between the main channel and channel for drift and raft), and indication of erosion of the riverbank in the year 1896 ("Anbrüche des Vorlands 8/9. III. 1896"). Panel B: overlay of study site as a reference to modern situation.

#### References

Álvarez-Vázquez, M.A., Hošek, M., Elznicová, J., Pacina, J., Hron, K., Fa´cevicová, K., Talská, R., Bábek, O., and Grygar, T. M.: Separation of geochemical signals in fluvial sediments: New approaches to grain-size control and anthropogenic contamination, Applied Geochemistry, 123, https://doi.org/10.1016/j.apgeochem.2020.104791, 2020.

Degering, D. and Degering, A.: Change is the only constant - time-dependent dose rates in luminescence dating, Quaternary Geochronology, 58, https://doi.org/10.1016/j.quageo.2020.101074, 2020.

Fuchs, M., Fischer, M., and Reverman, R.: Colluvial and alluvial sediment archives temporally resolved by OSL dating: Implications for reconstructing soil erosion, Quaternary Geochronology, 5, 269–273, https://doi.org/10.1016/j.quageo.2009.01.006, 2010.

Fuchs, M. C., Kreutzer, S., Burow, C., Dietze, M., Fischer, M., Schmidt, C., and Fuchs, M.: Data processing in luminescence dating analysis: An exemplary workflow using the R package 'Luminescence', Quaternary International, 362, 8–13, https://doi.org/10.1016/j.quaint.2014.06.034, 2015.

Govindaraju, K.: Compilation of working values and sample description for 383 geostandards, Geostandards Newsletter, 18, 1–158, https://doi.org/10.1046/j.1365-2494.1998.53202081.x-i1, 1994.

Kicińska, A., Pomykała, R., and Izquierdo-Diaz, M.: Changes in soil pH and mobility of heavy metals in contaminated soils, European Journal of Soil Science, 73, https://doi.org/10.1111/ejss.13203, 2022.

Knausenberger, G.: Der Kinzigtäler Bergbau - eine Zusammenfassung über Gesichertes und Ungesichertes, Die Ortenau, 2001.

Lang, A. and Honscheidt, S.: Age and source of colluvial sediments at Vaihingen-Enz, Germany, Catena, 38, 89–107, www.elsevier.comrlocatercatena, 1999.

Lang, A., Bork, H. R., Mäckel, R., Preston, N., Wunderlich, J., and Dikau, R.: Changes in sediment flux and storage within a fluvial system: Some examples from the Rhine catchment, Hydrological Processes, 17, 3321–3334, https://doi.org/10.1002/hyp.1389, 2003.

Larsen, A., Bork, H. R., Fuelling, A., Fuchs, M., and Larsen, J. R.: The processes and timing of sediment delivery from headwaters to the trunk stream of a Central European mountain gully catchment, Geomorphology, 201, 215–226, https://doi.org/10.1016/j.geomorph.2013.06.022, 2013.

LGRB: Landesamt für Geologie, Rohstoffe und Bergbau: Fachanwendungen und Fachthemen - Geologie - Geologische Übersichtskarte 1:300000 (GÜK300) - GÜK300: Geologische Einheiten; https://maps.lgrb-bw.de/, 2024.

Mandiwana, K. L. and Panichev, N.: The leaching of vanadium(V) in soil due to the presence of atmospheric carbon dioxide and ammonia, Journal of Hazardous Materials, 170, 1260–1263, https://doi.org/10.1016/j.jhazmat.2009.05.061, 2009.

Oyewo, O. A., Adeniyi, A., Bopape, M. F., and Onyango, M. S.: Heavy metal mobility in surface water and soil, climate change, and soil interactions, pp. 51–88, Elsevier, ISBN 9780128180327, https://doi.org/10.1016/B978-0-12-818032-7.00004-7, 2020.

Preusser, F., Degering, D., Fülling, A., and Miocic, J.: Complex Dose Rate Calculations in Luminescence Dating of Lacustrine and Palustrine Sediments from Niederweningen, Northern Switzerland, Geochronometria, 50, 28–49, https://doi.org/10.2478/geochr-2023-0003, 2023.

Ramsey, C. B.: Bayesian analysis of radiocarbon dates, Radiocarbon, 51, 337–360, https://doi.org/10.1017/s0033822200033865, 2009.

Rommens, T., Verstraeten, G., Bogman, P., Peeters, I., Poesen, J., Govers, G., Rompaey, A. V., and Lang, A.: Holocene alluvial sediment storage in a small river catchment in the loess area of central Belgium, Geomorphology, 77, 187–201,

https://doi.org/10.1016/j.geomorph.2006.01.028, 2006.

Trimble, S.: Decreased rates of alluvial sediment storage in the Coon Creek Basin, Wisconsin, 1975–93, Science, 285, 1244–1246, https://doi.org/10.1126/science.285.5431.124, 1999.

Verstraeten, G., Broothaerts, N., Loo, M. V., Notebaert, B., D'Haen, K., Dusar, B., and Brue, H. D.: Variability in fluvial geomorphic response to anthropogenic disturbance, Geomorphology, 294, 20–39, https://doi.org/10.1016/j.geomorph.2017.03.027, 2017.

Walling, D.E., and He, Q.: The spatial variability of overbank sedimentation on river floodplains, Geomorphology, 24, 209-223, https://doi.org/10.1016/S0169-555X(98)00017-8, 1998.

Weber, A. and Lehmkuhl, F.: Mixed response of trace element concentrations in fluvial sediments to a flash flood in a former mining area, Environmental Sciences Europe, 36, https://doi.org/10.1186/s12302-024-00926-5, 2024.